





Review

Cleaning Up Metal Contamination after Decades of Energy Production and Manufacturing: Reviewing the Value in Use of Biochars for a Sustainable Future

Priyanka ^{1,2,†}, Isobel E. Wood ^{1,3,†} , Amthal Al-Gailani ¹, Ben W. Kolosz ^{3,*} , Kin Wai Cheah ⁴ , Devika Vashisht ², Surinder K. Mehta ^{2,5} and Martin J. Taylor ^{1,*} 

¹ School of Engineering, Chemical Engineering, University of Hull, Cottingham Road, Hull HU6 7RX, UK; a.z.al-gailani@hull.ac.uk (A.A.-G.)

² Department of Chemistry and Centre for Advanced Studies in Chemistry, Panjab University, Chandigarh 160014, India; skmehta@pu.ac.in (S.K.M.)

³ Energy and Environment Institute, University of Hull, Cottingham Road, Hull HU6 7RX, UK

⁴ School of Computing, Engineering & Digital Technologies, Teesside University, Borough Road, Middlesbrough TS1 3BA, UK; k.cheah@tees.ac.uk

⁵ Department of Chemistry, University of Ladakh, Kargil 194103, India

* Correspondence: b.w.kolosz@hull.ac.uk (B.W.K.); martin.taylor@hull.ac.uk (M.J.T.)

† These authors contributed equally to this work.

Abstract: The lasting impact of ancestral energy production operations and global manufacturing has not only generated substantial CO₂ emissions, but it has also led to the release of metal-based pollutants into Earth's water bodies. As we continue to engineer, mine (coal and metals), and now bore into geothermal wells/fracking sites for alternative energy sources, we continue to contaminate drinking water supplies with heavy metals through infiltration and diffusion, limiting progress towards achieving Sustainable Development Goals 3 (Sustainable Development Goal 3: Good health and well-being), 6 (Sustainable Development Goal 6: Clean water and sanitation), 14 (Sustainable Development Goal 14: Life below water), and 15 (Sustainable Development Goal 15: Life on land). This review shows how the research community has designed and developed mesoporous biochars with customizable pore systems, as well as functionalized biochars, to extract various heavy metals from water sources. This article investigates how biochar materials (non-activated, activated, functionalized, or hybrid structures) can be adapted to suit their purpose, highlighting their recyclability/regeneration and performance when remediating metal-based pollution in place of conventional activated carbons. By utilizing the wider circular economy, "waste-derived" carbonaceous materials will play a pivotal role in water purification for both the developed/developing world, where mining and heavy manufacturing generate the most substantial contribution to water pollution. This review encompasses a wide range of global activities that generate increased heavy metal contamination to water supplies, as well as elucidates emerging technologies that can augment environmental remediation activities, improving the quality of life and standard of living for all.

Keywords: biochar; water remediation; waste from energy production; heavy metal removal; life cycle analysis; Sustainable Development Goals



Citation: Priyanka; Wood, I.E.; Al-Gailani, A.; Kolosz, B.W.; Cheah, K.W.; Vashisht, D.; Mehta, S.K.; Taylor, M.J. Cleaning Up Metal Contamination after Decades of Energy Production and Manufacturing: Reviewing the Value in Use of Biochars for a Sustainable Future. *Sustainability* **2024**, *16*, 8838. <https://doi.org/10.3390/su16208838>

Academic Editor: Andrea Nicolini

Received: 4 September 2024

Revised: 1 October 2024

Accepted: 9 October 2024

Published: 12 October 2024



Copyright: © 2024 by the authors. Licensee MDPI, Basel, Switzerland. This article is an open access article distributed under the terms and conditions of the Creative Commons Attribution (CC BY) license (<https://creativecommons.org/licenses/by/4.0/>).

1. Introduction

Research into the field of sustainability is driven by the United Nation's Sustainable Development Goals (SDGs). The 17 goals are essential for true global prosperity and will improve the quality of life and the standard of living for all humankind, as well as tackle climate change directly (SDG 13). However, in our mission to stem and, in some cases, reverse climatologic disaster, spurred on by our nonchalant release of greenhouse gases (GHGs), we have started to take full stock of the global environmental damage. Over 50.6 GtCO₂eq^{−1} of GHG emissions were released in 2022 [1], 30.6 GtCO₂eq^{−1} specifically

related to carbon dioxide (CO₂) [2] and hard-to-decarbonize sectors, including energy production and manufacturing. To limit the further release of CO₂ during energy production, countries have adopted Net-Zero targets. For some countries, this involves the direct capture and storage of ancestral CO₂ from the atmosphere to reduce the current concentrations (Carbon Dioxide Removal, or CDR). True Net Zero is where a country completely negates the release of GHGs produced by human activity (anthropogenic), focused on the reduction in and elimination of fossil-fueled power production. As a result, the focus has now switched to renewable/alternative forms of energy production [3]. These include nuclear, wind, solar, and geothermal energy, and, in some cases, fracking for shale oil/gas (SDG 7). Fracking, unlike other energy sources, is a carbon-intensive process which releases CO₂ through the extraction process unless adequate carbon capture and storage (CCS) technologies can be applied.

Although it is well documented that ocean acidification is taking place through the diffusion of CO₂ into the oceans, other water systems are being polluted by secondary, inorganic waste streams. It is our duty, aligning with SDGs 6, 3, 14 and 15, to maintain our water systems and prevent the toxic buildup of heavy metals, which can lead to adverse health effects on humans, animals and on a wider scale, natural biodiversity [4]. Some places possess elevated levels of heavy metals, depending on where they are situated or through their own mining operations [5]. By 2030, we need to triple our renewable energy supply [6], and with global surges in energy demands and the extensive amount of land required to accommodate growing populations, there is an escalating risk of heavy metal pollutants being released into more locations due to increased activity in the energy production/storage industry.

Water pollution is caused by the discharge of toxic derivatives such as heavy metals into water sources, as well as through ground infiltration from standing water that can migrate to larger water bodies and tributaries [7]. These metallic contaminants are defined as entities that are five times denser than a molecule of water [5], and due to their often-high solubility in water, living organisms can ingest and absorb them into their bloodstreams, where they can accumulate to reach dangerous levels [7]. Waste streams emitted from industries such as coal combustion (directly for energy or through the production of coke), metal plating/milling (shaving or swarf particulates), pesticide usage, battery production and mining can be associated with the release of heavy metals [7–10]. There are ten heavy metals identified as major public health hazards, including lead, arsenic, cadmium, mercury and chromium, attributed to their associated health effects such as cancer, dermatitis, circulatory failure, organ failure and nervous system damage [4].

The current methods identified for water treatment comprise chemical precipitation, contaminant adsorption into porous filters, phytoremediation and reverse osmosis [8,9]. However, these methods have been found to have high costs, relatively long operating times, and potentially poor removal efficiencies and can cause secondary pollutants during the process, which require further treatment. The use of a bio-adsorbent such as biochar is an appealing method as it can be derived from organic waste streams, lowering its associated costs and making it more environmentally appealing, as well as being a carbon neutral material (avoiding the potential release of CO₂ into the atmosphere), in comparison to conventional adsorbents such as fossil-derived activated carbons [11]. Biochars also have great customizable structures and tunable surface functional groups that can be added during production or post-processing. It is also feasible to alter the physicochemical properties of biochar, such as pore volume and surface area, to further increase its removal efficiency through the selection of feedstock, additives and pyrolysis temperature during synthesis [7,9,12,13].

This review explores a broad range of knowledge and demonstrates how biochars, including bare biochars, surface-functionalized biochars, and structured biochars with enhanced pore networks, can be effectively used for environmental remediation. Specifically, the focus is on addressing metal release resulting from energy production (past and emerging), mining and manufacturing industries. This review also contextualizes the

relevance of biochar to Net-Zero targets and carbon dioxide sequestration, alongside metal adsorption to demonstrate its true multifunctionality, as a direct replacement for tried and tested, traditional activated carbon from non-renewable sources. Moreover, this review highlights routes to generate selective adsorbents through biochar functionalization as a means of targeting specific contaminants/pollutants, leading to the kinetics behind the potential adsorption process as well as reaction pathways.

2. Biochar, a Sustainable Carbonaceous Material

Biochar is a carbon-rich, solid substance created by the thermal transformation (deoxygenation) of biomass residues in an oxygen-deficient atmosphere [14–16]. Biochars possess the unique ability to improve the surrounding soil environment. Biochars are born through the thermochemical transformation of lignocellulosic biomass waste streams during energy/fuel production, as a primary product from pyrolysis, or as a secondary product from gasification [11], in which the produced biochars are carbon-rich. Depending on its chemical makeup, biochar is more durable than its original pre-processed biomass waste state, being more difficult to decompose than usual plant matter due to the removal of volatile components [17–19]. Biochar may, however, not be as stable as microbial remnants in soil or soil organic carbon (SOC), and more work needs to be carried out to understand its full effects on the environment, as well as the mechanisms and timescales of oxidation [20–22]. Over 50% of studies focusing on biochar as a soil amendment have taken place in highly controlled laboratory-type conditions involving the use of a greenhouse to generate a model environment [23]. More research must be conducted across a range of different soil types and varying timescales. In addition, it is imperative that further experiments are carried out in order to generate long-term data that can help us understand the behavior of biochar carbon pools in soil [24]. To optimize the impact of biochar applications on soil carbon sequestration, further analyses are needed on the impact of biochar on climate, crops management, soil factors and other GHGs. It is therefore hoped that this timely review illuminates the research community on the latest advancements in biochar as a multifunctional remediation and CDR technology [22].

Biochar can be produced from a wide range of waste feedstocks, which all alter the physicochemical properties differently. These range from municipal waste, forest residues, agricultural waste and more, and the use of these tertiary or quaternary sources can resolve concerns surrounding the food vs. fuel debate [25,26]. In addition, utilizing waste as a feedstock can support the world waste problem or SDG 12.3, which aims to reduce food waste by 50% [27]. For example, approximately 931 Mt of food waste was generated in 2019, including waste from the food industry, households, and retail establishments, which could be used as a feedstock for biochar [27].

A study completed by Zilberman et al. reviewed how biochar can be implemented alongside biofuel production [28]. It considered biochar production using the residual crop waste of a biofuel crop, such as corn stover, in parallel to the production of biofuel from corn grain, and how this process could be considered carbon-neutral. As biochar can also be used to improve soil quality, it can also improve the crop's yield within the same land usage. One of the concerns of the food vs. fuel debate is the indirect impact of land use. If it is possible to increase the yield of crops on the same land area, this can have a positive impact. If in the United States of America, biochar could be used to increase the yield of corn, soybeans, and wheat by 1% through soil improvement, it would be possible to reduce the global land use by 0.06% [28].

Relevance to Net Zero

Biochar arguably constitutes the proposed “Scope 4” of the carbon cycle [29], indicating that it can be considered either as an avoided emission by reducing the decomposition of biomass as a standalone amendment, or it can be produced as part of a CDR portfolio. The potential climate removal estimates currently range between 1.1 and 3.3 GtCO₂eq/yr by 2030, albeit with a high degree of uncertainty [30–32]. However, this range is very

uncertain and new mechanistic modeling approaches that account for the complexity of biochar and the external environment are necessary to assist with making such predictions more accurate, particularly in terms of soil carbon sequestration and net GHGs. Process-based models are mandatory to understand complex interactions. Long-term field trials of different soils, environments and supervisory approaches are essential. LCAs of biochar should possess sufficient fidelity to include the persistence and carbon storage value of the biochar itself, the amount of feedstock that is released as CO₂ during production, as well as the sequestration potential and agronomic benefits of the feedstock (pyrolysis or natural soil amendment), agricultural productivity and soil trace gas emissions in the form of nitrous oxide or methane [33,34]. According to Matušík and co-workers, a comparison of the biochar performances across studies is extremely difficult due to the significant methodological differences in their syntheses/compositions, which indicates that LCA development protocols that specifically handle biochar practices should be implemented to improve such comparisons [35]. Therefore, new, more sophisticated models need to be developed to quantify the complex interactions within the local soil substrates so that the potential impact on climate change mitigation can be better understood [36]. Process-based models are mandatory and must be calibrated so that they can determine biochar's influence on crop yields and the wider environment. Biochar production through biomass energy with carbon capture and storage (BECCS) is possible if biomass growth and biochar production are also included within the lifecycle analysis (LCA) boundary [36]. Biochar decomposes much more slowly than biomass, which means that embedded photosynthetic CO₂ is released at a much slower rate [37–39].

Biochar also possesses the ability to stabilize other soil amendments where SOC matter has been added to soil, compost being a common example of a typical additive [40]. In a way not too dissimilar from the behavior of inert organic matter (IOM), which makes up a fraction of soils globally, it can form long-term carbon pools in addition to soil fertility and soil quality benefits. It may even be possible to offer additional benefits including, but not limited to enhancing microbial activity [41], improving water capacity/retention [42], nutrient availability [43,44], reducing the risk of plant disease [45] and the remediation of contaminated soils through physisorption and chemisorption mechanisms [46,47]. Soil quality can be enhanced by elevating the pH; therefore, biochar possesses the latent ability to improve the yields of crops [23,48,49], in addition to improving soil carbon storage through the return of carbon to the soil [50]. Ultimately, biochar can provide improved carbon sequestration through the upscaling of biomass waste usage, especially in the thermochemical waste-to-energy process [40].

3. Origins of Biochar—Waste Resources

Biomass waste feedstocks are complex, containing both organic and inorganic components and derived from recently living solid substances that are naturally occurring. A variety of wastes, such as wood surplus, agricultural crop leftovers, organic waste, animal compost and forestry residues, have been considered “biomass” because they contain a blend of organic and inorganic components. Feedstocks can be divided into primary, secondary and tertiary biomass, as well as organic, inorganic and fluid biomass, based on a variety of factors [51]. According to Vassilev et al., biomass can be classed as either naturally occurring or manmade. Anthropogenic biomass is created by the processing of natural matter, whereas natural biomass has a natural origin [52]. The two categories of available biomass are lignocellulosic biomass and non-lignocellulosic biomass. Lignocellulosic biomass is a type of plant-based material composed mainly of cellulose, hemicellulose, and lignin, while non-lignocellulosic biomass refers to organic material that lacks significant amounts of cellulose and lignin. Agricultural waste, forest waste, and others are examples of lignocellulosic biomass, whereas sewage sludge, manure, and animal bones are non-lignocellulosic biomass [53].

Aquatic biomass options such as green algae, blue algae and fungi are another category of biomass, considered as the third generation of bio-renewable feedstocks. Industrial waste involves waste from industries such as sugarcane residues and paper sludges; in addition to producing energy, the problem of disposing of these waste materials is somewhat alleviated when they are processed and turned into valuable energy products. It might be possible to tackle waste and promote environmental sustainability by turning low-value materials or waste streams into biochar that have minimal usage elsewhere. The primary goal of using this biomass is to eliminate the risk of climate issues triggered by the discharge of damaging GHGs [54]. The core organic components that make up lignocellulosic biomass are cellulose, hemicellulose and lignin, as shown in Figure 1 [55]. Cellulose is a key component of plant cell walls that is made up of glucose molecules, while hemicellulose provides support and contains various sugar monomers. Lignin adds rigidity and resistance to degradation in plant cell walls.

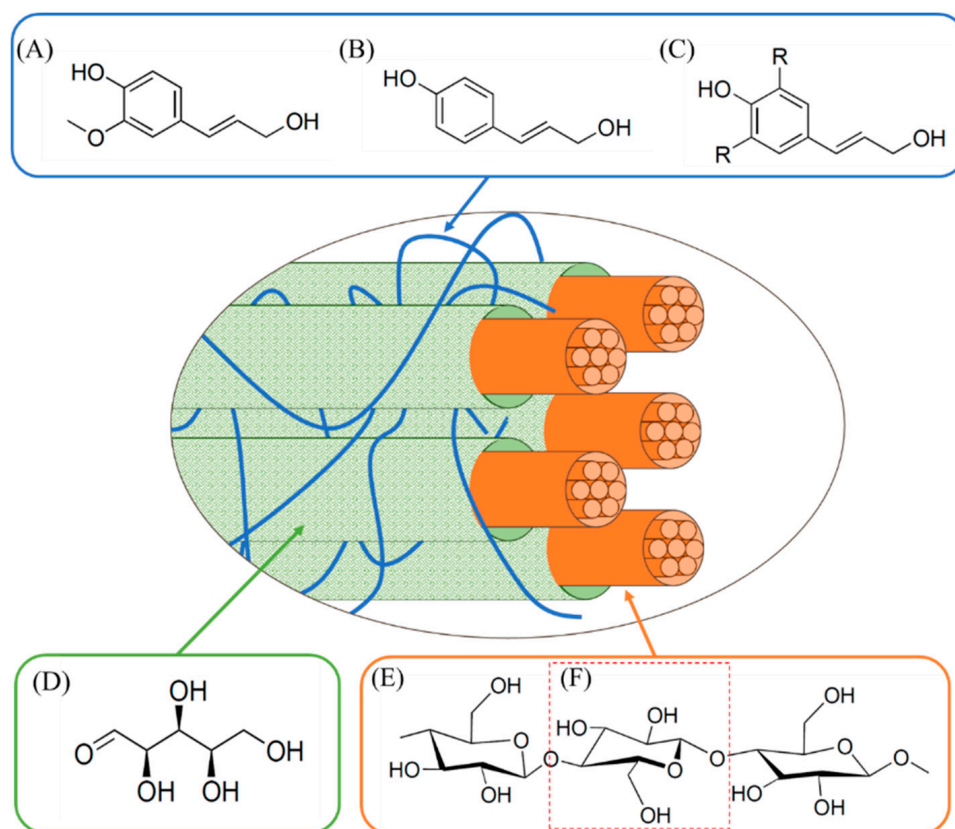


Figure 1. The structure of the core organic components in lignocellulosic biomass includes lignin, represented as three different hydroxycinnamyl alcohols (blue box): (A) coniferyl alcohol, (B) p-coumaryl alcohol, and (C) sinapyl alcohol. Hemicellulose (green box) represented as (D) xylose, a monomer found in xylan, and cellulose (orange box) depicted as (E) a cellulose polymer and (F) an individual glucose monomer. Adapted from [56–58].

Since cellulose and lignin components are difficult to break at moderate temperatures, lignocellulosic biomass requires a higher temperature and often a longer residence time. This is due to the lignin polymeric backbone supporting the superstructure of the lignocellulosic matrix [59]. At a temperature of 250–300 °C, hemicellulose and then cellulose are thermally decomposed, starting through the depolymerization of hemicellulose and pectin, which is a polysaccharide [60]. This is followed by cellulose thermally decomposing shortly afterwards, thus starting the carbonization process to produce biochar. The final organic component, lignin, has been seen to decompose within a broad temperature range of 160–900 °C. However, one can observe large mass losses for lignocellulosic wastes at ~400 °C, which is considered the beginning of pyrolysis [11,61]. For emerging feedstocks

such as microalgae or sludges often found in wastewater, the carbonization process has been seen to operate at lower temperatures (180–350 °C) because the lignin content of these two organic precursors is lower than the “traditional” feedstock options used [62,63].

Thermochemical Production of Biochars

Pyrolysis is a thermochemical conversion technique operated in an oxygen-free environment at temperatures generally ranging from 300 to 900 °C [64]. The process uses heat to decompose the biomass waste feedstock into value-added chemicals, in the presence or absence of a catalyst to maximize product selectivity. A portion of the biomass (depending on the method used) is also converted to biochar through thermochemical reactions, in addition to their primary/secondary products [65].

Pyrolysis is described as the thermal degradation of organic waste. When lignocellulosic biomass is pyrolyzed, the organic components undergo crosslinking, fragmentation and depolymerization reactions, resulting in the generation of solid (biochar), liquid (bio-oil), and gaseous (syngas) products, depending on the rate of heating used [14,66]. Lignin is the most challenging to decompose due to its highly variable chemical structure (Figure 1). As a result, this component may undergo different kinds of mechanisms when pyrolysis takes place [67]. The yield of the product is determined by whether the pyrolysis is “slow” or “fast”, with a third known as “flash”. These two processes can be distinguished by characteristics such as the heating rate and the feedstock’s residence time [15]. Slow heating rates and lengthy residence durations result in slow pyrolysis, which primarily yields solid material (biochar); typically, low heating rates are used for this pyrolysis approach at <5 °C/min [68].

Although biochar is a dominant product produced, there are still oil and tar residues adsorbed onto the surface and present in pyrolysis vapors (gas-phase products). These often condense in the colder regions of the reactor, forming tar-like residues [69]. The general product mix for slow pyrolysis is seen as ~35% biochar, ~30% condensable liquid, and ~35% syngas by mass, subject to the feedstock used, while fast pyrolysis produces ~12% biochar, ~75% bio-oil and ~13% producer gas [70].

4. Heavy Metals from Waste Supplies

Maintaining the global water supply is crucial, aligning with SDGs 6, 3, 14 and 15. Sediment pollution caused by heavy metals threatens human life and the environment, due to their stability, non-biodegradability, toxicity and ability to accumulate within the food chain [71]. With most metals contaminating water from industrial production, the pollutants are variable both in terms of the element and concentration in the environment.

4.1. Mines

Metals exist within active and around abandoned coal mines in contaminated soil, mine tailings and wastewater [72,73] (Table 1). Metals are hazardous to human health and the wider ecosystem, leading to the contamination of surrounding groundwaters, particularly in the presence of acid compounds, and they therefore require treatment in the form of mine remediation practices. Mine tailings, depending on the parent mine’s usage include multiple metals, tailing ponds and coal mine spoils, which are the materials remaining following the extraction of ores, typically characterized by high concentrations of heavy metals [74]. The mobility of heavy metals in soils is influenced by parameters such as the ionic strength, pH and organic matter content. These factors play a significant role in affecting the adsorption and dissolution processes. This has been shown in piece of work where it was found that as the pH decreased, the concentration solution of Cd, Cu and Pb of sludge-amended soils increased. Therefore, the soil characteristics increase the risk of metal leaching leading to infiltration through the ground towards waterways and tributaries [75].

Table 1 shows some of the types and concentrations of heavy metals identified in locations near mines identified in the wider literature. Coal mining sites in different locations were reviewed to compare their concentration levels of heavy metals. It was found in Anhui Province (China) that surrounding the coal mining site, the elements observed were in the following order of concentration: Fe > Cr > Mn > Zn > As > Pb > Cu > Cd [76]. In the Damodar River Basin (India), the heavy metals post mining were in the concentration order: Fe > Zn > Al > Mn > Cr > Ni > Se > Cu > Pb > Cd > As [77]. The surface water concentrations of heavy metals near mining sites in South Korea (Sangdeok) were in the following order: Mn > Zn > Cu. Manganese was in high concentrations similar to those of the other sites and copper was on the lower end [78]. The heavy metal concentrations in the water systems of an iron mining site in northeast Morocco were found to be in the following order: Fe > Cu > Zn > Ni > As > Cr > Cd > Pb. Comparable to the coal mining sites reviewed, the heavy metal with the highest concentration identified was iron. However, copper was the heavy metal with the second highest concentration, unlike the coal mining locations [79].

Table 1. Different types of heavy metals found in water sources near mining sites.

Mining	Location	Heavy Metal	Concentration	Unit	References
Coal	Anhui Province, China	Cd	0.95–58.25	µg/L	[76]
		Cr	38.99–982.60		
		As	3.61–163.80		
		Mn	23.02–524.27		
		Fe	93.10–1050.84		
		Cu	2.40–68.27		
		Zn	4.52–257.30		
		Pb	0.69–72.84		
Anthracite coal	Sangdeok, Gangwon, South Korea	As	0	µg/L	[78]
		Cd	0		
		Cu	0–9		
		Mn	1–2060		
		Pb	0		
		Zn	3–1818		
Iron	Ouixane mining district, Morocco	Zn	0.08–38.5	mg/L	[79]
		Cu	≤0.01–101.51		
		Fe	≤0.01–>>1000		
		Ni	≤0.01–8.05		
		As	≤0.01–2.49		
		Pb	0.01–0.24		
		Cd	≤0.01–0.26		
		Cr	≤0.01–0.32		

Table 1. Cont.

Mining	Location	Heavy Metal	Concentration	Unit	References
Coal	Damodar River Basin, India	Fe	130.6–601.3	µg/L	[77]
		Mn	2.02–23.6		
		Cu	1.1–5.6		
		Pb	0.01–2.01		
		Zn	3.2–89.2		
		Ni	2.1–11.6		
		As	0.12–0.43		
		Se	2.4–6.6		
		Al	3.4–52.6		
		Cd	0.04–2.0		
		Cr	1.1–14.4		
Gold	Kokoteasua, Ghana	As	<0.05	mg/L	[80]
		Cu	<0.02		
		Fe	<0.1		
		Mn	0.17		
		Pb	<0.02		
		Zn	<0.05		
Lignite	Zazari, Greece	As	0.08–1.38	µg/L	[81]
		Cr	1.10–2.10		
		Zn	2.00–359		
		Fe	150–810		
Silver	Creede, CO, United States	Cd	32.9	mg/kg *	[82]
		Cu	102		
		Pb	4370		
		Zn	5080		
Not specified	New South Wales, Australia	Cd	0.58	mg/L	[83]
		Cu	2.28		
Zinc/lead ore	South East Spain	Fe	90,700	mg/kg	[84]
		S	19,400		
		Zn	13,800		
		As	1510		
		Cu	435		
		Sb	156		
		Co	79		

Table 1. Cont.

Mining	Location	Heavy Metal	Concentration	Unit	References
Sulfide minerals	Iberian Pyrite Belt, Spain	Fe	23.48	% **	[85]
		Si	14.66		
		Al	3.49		
		S	2.25		
		Mg	2.07		
		Ca	1.04		
		Cu	0.941		
		Zn	0.313		
		Ti	0.165		
		K	0.210		
		Mn	0.120		
		As	0.102		
		Sb	0.0491		
		Pb	0.0396		
		Co	0.0301		

* Concentrations were taken from soils rather than water samples; ** values are in content % of the mine waste sample.

This demonstrates some of the variability in metal contamination released from mining activities and location. However, a common theme shown by the examples mentioned is the presence of Cr, Cd, arsenic and Pb. These elements are very toxic to humans, animals, and broader biodiversity, where there are already some restrictions in place globally for the release of heavy toxic metals into the environment through landfills. One such example is Cr toxicity. In plants, Cr can lead to reduced plant growth, as it affects plants' mineral nutrition, water retention, and ability to photosynthesize, thus threatening food chains. In humans and animals, studies have found that Cr causes acute poisoning by inducing oxidative stress in cells, leading to DNA damage and gene mutation, showing physical effects such as vomiting, blood loss and cardiovascular shock [86,87]. Ghosh and Maiti suggested that the selection of charcoal trees for biochar production, which are a type of rapid growing tree that can be cultivated near mining sites, can aid in the reduction in lifecycle emissions, mainly because there is less reliance on transport, as well as reduce the uncertainty of the charcoal availability [73]. Such trees also grow rapidly, possessing superior lignin and holocellulose content, resulting in a higher-quality biochar. Wildfires, air pollution and particulates from burning such wood are also reduced. Applying biochar in pits can immobilize metals, reduce application rates and encourage plant growth. Phytoremediator biomass removal technologies will help mitigate heavy metal-induced toxicity [73].

Biochar has a proven ability to increase soil pH, restricting the movement of some metals. For example, Beesley and Marmiroli carried out an experiment on contaminated soils which showed a 300-fold reduction in Cd, as well as a 45-fold reduction in Zn, through a column leaching experiment and scanning electron microanalysis [88]. In another study, Puga et al. carried out an experiment using biochar derived from sugarcane waste for the removal of Cd, Pb and Zn present in leachates from a mine in Vazante, Minas Gerais state, Brazil [72]. The work found that the biochar extracted more Cd from the leachate due to its mobility through the adsorbent, whereas Pb was removed at a lower concentration.

Ippolito et al. carried out a study to determine whether biochars produced from feedstocks close to a local contaminated silver mine (Creede, CO) could improve upon the reduction in metals in the leachates [82]. Their work proved that it was possible to utilize local feedstocks such as pine beetle-killed lodgepole pine and tamarisk for the production

of biochar. Soils containing Cd, Cu, Pb and Zn metals were exposed to increasing quantities of the produced biochar (equal to 0, 5, 10, or 15% by weight) in test tubes, where 30 mL of 0.01 M CaCl was added and the samples centrifuged. It was found that the pH of the soils in the areas dosed with biochar increased from 3.97 to 7.49, with a 55–100% reduction in the metal bioavailability.

Bandara et al. carried out a study where biochars were produced from a commercial-scale mobile pyrolyzer to reduce the metal contamination in mine wastewaters in New South Wales, Australia, with a low pH of 3.2 [83]. The biochars were derived from canola shoots, poultry litter, sugar-gum wood, vetch, lucerne shoots and wheat straw. The poultry litter-derived biochar removed Cd and Cu from the mine wastewater, bringing the concentration down to the appropriate levels (0.003 and 2 mg/L, respectively) stipulated by the World Health Organization, highlighting that feedstock selection is important when attempting to mitigate multiple metal types. The lucerne biochar had the highest sorption capacity of Cd (II) (6.28 mg g⁻¹), and the vetch biochar had the highest Cu (II) sorption capacity (18.0 mg g⁻¹) at pH 5.5 (Table 1). In another approach, Chen et al. assessed how biochar from walnut shells in filled constructed wetlands could remove multiple metal types through adsorption and biotic removal routes [89]. High capacities of metal binding and acid neutralization were achieved, including improved plant growth and metal mitigation from the plant roots to the shoots.

Alvarez et al. carried out a study on an abandoned zinc/lead mine in the southeast of Spain [84]. The pyrolysis of pruning waste provided two biochar–Fe composites (BM–Fe through pyrolysis and a hydrochar named HM–Fe) through the impregnation of 5 wt% ferric sulfate. These materials were used to trial the removal of Zn, Cu, As and Sb from water. Unfortunately, Zn recovery was unaltered, however, as leaching was reduced significantly. Barragán-Mantilla et al. carried out tests on mining waste in the Iberian Pyrite Belt (Spain) using biochar derived from sugarcane bagasse [85]. In total, Cu and Zn extraction was accomplished using an adsorbent produced at 750 °C, with removal values of 82.9% and 98.1%, respectively, with materials showing non-phytotoxicity. More attention needs to be given to the net removal cost of biochar applied within abandoned mining areas to remove such metals.

Biochar has demonstrated a strong capacity to immobilize heavy metals, reducing their bioavailability and movement in soils, as seen in the work of Beesley and Marmiroli [88] and Puga et al. [72]. Feedstock selection is also crucial, with different biochar sources exhibiting varying levels of effectiveness for specific metals. For instance, Bandara et al. [83] highlighted the importance of choosing appropriate feedstocks, such as lucerne and vetch, to target contaminants like Cd and Cu. Additionally, the utilization of local resources for biochar production, as noted by Ippolito et al. [82], offers a practical and sustainable approach to soil remediation. Furthermore, modifying biochar with metals like Fe enables the selective removal of certain heavy metals, such as As, while showing less efficiency for others, like Zn, as demonstrated in the study by Alvarez et al. [84].

4.2. Manufacturing

Manufacturing encompasses a variety of sectors and activities; however, to simplify it, we can define it as “establishments engaged in the mechanical, physical, or chemical transformation of materials, substances, or components into new products” [90]. This includes the production of materials, apparatuses, and chemicals for the energy industry, such as steel for distillation towers, or batteries for energy storage. Manufacturing industries also remain heavily reliant on fossil fuels, due to being energy-intensive processes, contributing to 75%, 20%, and 44% of the global annual coal, oil, and natural gas consumption, respectively [91]. The waste streams of different manufacturing plants also contribute to the deposition of heavy metal pollutants into their surrounding environments.

A study looked at the heavy metal pollution of urban aquatic environments in Ma’anshan, China, a major steel producing area. Samples were taken from the Yushan River watershed, where the intensive steel industry activities are located. Their findings

showed, overall, that in the steel industry-impacted areas, there were higher levels of Cd, Cr, Cu, Pb and Zn compared with a control sample; however, Cd and Zn had the highest levels of accumulation [71].

Research carried out by Liu et al. looked at the heavy metal concentration in the Liao River Basin (Manchuria, China), which is infringed on by a multitude of different industries, including chemical, petrochemical, pharmaceutical, metallurgical and dyeing industries [92]. The average background levels of heavy metals identified in the Liao River Basin (LRB) can be found in Table 2 and were all higher than previously quantified in 1998. As heavy metals enter and traverse water systems, they undergo transformations such as dissolution, precipitation, sorption and complexation, where they are transported across long distances under hydrodynamic forces, until they coalesce into sediment. Consequently, the presence and diversity of the heavy metals identified in the LRB can be attributed to the numerous and various manufacturing activities around the subject area. Although, it may be possible to establish a correlation between an elevated concentration of a specific heavy metal and the proximity of a particular manufacturing site. For example, it was identified that in the upper stream of the LRB, there are higher concentrations of Hg in comparison to other test areas, which the researchers linked to the closer proximity to mechanical, chemical and metallurgical industries, whereas within the Tieling and Shenyang areas of the LRB, it was noted that electroplating, metallurgical and machine manufacturing industries were the most prominent, and it was also where the highest levels of Cu were measured [92].

Hsinchu Science Park comprises around 450 companies, serving as a hub for the global manufacturing of semiconductors, electronics and optoelectronics. The daily volume of wastewater generated is ~105,000 tonnes, with an average of 7.1 mg/L of suspended particles, which is treated and then released into the Keya stream (Liberia). The researchers found that although the wastewater is treated, the levels of heavy metals, including Cu, Zn, and Ni, were 2–10 times higher than those at the early stages of the Hsinchu Science Park operation. Although the majority of heavy metals were within the national water quality standards, the levels of Ag, Zn, Cu, As and Ni actually reached or exceeded the international sediment quality guidelines [93], meaning that further improvement is needed for water treatment from manufacturing industries to reduce the impact of heavy metal pollutants found in nearby water systems.

Table 2. Types and concentrations of heavy metals found in water sources around manufacturing sites.

Manufacturing	Location	Heavy Metals	Concentrations	Units	References
Steel production	Ma'anshan China	Cd	0.42–15.79	mg/kg	[71]
		Cr	66.89–352.08		
		Cu	22.01–133.37		
		Ni	22.66–50.80		
		Pb	14.66–264.37		
		Zn	73.20–2707.46		
		Cd	7.60–18.92 *		
		Fe	2165.68–27,069.10 *		
		Mn	638.9–1751.28 *		
		Cr	187.6–1855.26 *		
		Zn	325.42–876.82 *		
		As	0.01–0.72 *		

Table 2. Cont.

Manufacturing	Location	Heavy Metals	Concentrations	Units	References
Multiple (chemical, petrochemical, pharmaceutical, metallurgical, dyeing, etc.)	Liao River Basin (LRB), China	Cr	32.6–60	mg/kg	[92]
		Cu	11.1–21		
		Ni	13.1–27		
		Pb	16.3–23		
		Zn	37.8–96		
	Tuticorin industrial zone, India	Mn	0.029–1.316 *	mg/L	[94]
		Cu	0.001–0.068 *		
		Fe	0.007–5.649 *		
		Cr	0.001–0.184 *		
		Ni	0.015–0.757 *		
		Co	0.104–2.429 *		
		Pb	0.171–2.221 *		
		Zn	0.001–3.577 *		
Semiconductors, electronics and optoelectronics	Hsinchu Science Park, Taiwan	W	5.5–394	mg/L	[93]
		Cu	76–1462		
		Cd	1.0–12.6		
		Sn	6.6–319		
		Ag	0.8–9.7		
		Ga	30–78		
		Ni	45–118		
		As	13–28		
		Mo	1.1–13		
		Zn	214–311		
		Fe	0.9–5.4		
		V	3.7–126		
		Mn	52–637		
		Cr	66–131		
Cement	Oinyi River, Nigeria	Fe	200–208.6	mg/kg	[95]
		Mn	50.8–52.02		
		Zn	1.4–1.49		
		Cu	1.67–1.74		
		Cr	0.25–0.35		
		Cd	0.1–0.2		
		Pb	0.3–0.44		
		Ni	4.65–4.8		
Marble	Khaksar, Pakistan	Cu	2.2	mg/L	[96]
		Mn	0.91		
		Zi	3.03		
		As	0.012		

* Sediment values pre-monsoon.

Table 2 provides a view of a few types of manufacturing and the concentrations of heavy metals that can be associated with different regions.

4.3. Geothermal Fluids

The term “geothermal fluid” refers to hot water (brine) or steam derived from depths of a few meters to multiple kilometers beneath the Earth’s surface. The heat stored in geothermal fluids in shallow aquifers is derived from solar radiation, while the decay of mildly radioactive elements is responsible for the heat stored in deep aquifers [97].

Deep geothermal fluids contain dissolved solids, such as sodium chloride, bicarbonate, sulfate, and silica, with concentrations varying between 100 and 250,000 g/tonne in the Salton Sea. The chemical composition of geothermal fluids varies within and between the geothermal fields. In general, geothermal fluids are rich in heavy metals owing to the water–rock interactions in deep aquifers [98]. The concentration of metals increases with the geothermal spring temperatures due to the increasing rate of rock dissolution [99]. As a result, the concentrations of heavy metals in geothermal fluids are higher than those in groundwaters, estimated at 344 mg/L [100] and 20.2 mg/L [101], respectively. The primary use of geothermal fluids is power generation by extracting heat from the fluid by steam separation or a single-phase heat exchanger. As a result of fluid flashing in geothermal plants, the water becomes concentrated with different metals, including lead, arsenic, cadmium, chromium, zinc, copper, and mercury, which impose health and environmental impacts in cases of reinjection and leach out to surface and groundwaters or are recycled and reused for aboveground purposes. Figure 2 illustrates the primary uses of geothermal fluids, such as aquaculture, balneotherapy, snow melting and thermal health tourism.

The primary heavy metals present in geothermal fluids and their environmental and operational impacts are described in Table 3. The environmental effects of raw or reinjected geothermal fluids on soil and plants will only be discussed, as the treatment of geothermal water is still infeasible and energy-intensive. Therefore, the direct impact of heavy metals on health is not included in Table 3. The concentration column represents the mean concentrations of metals in geofluids at high (maximum limit) and moderate (minimum limit) temperatures [102].

Table 3. The impacts of different heavy metals from geothermal fluids.

Metal	Max. Permissible Limit (mg/L)	Concentration (mg/L)	Impact	References
Pb	0.01	0.092–65.4	In power plants, lead precipitates as lead sulfide/oxide in pipelines and flash separators from geothermal fluids with different enthalpies. The deposition of lead sulfide/oxide retards a plant’s capacity by blocking the pipes and valves. In addition, lead ions in geothermal brine react with iron in carbon steel pipes/units, causing galvanic corrosion and the precipitation of native lead (Pb ⁰).	[103,104]
			In agriculture, lead causes lower growth of seedlings, reduction in the growth of the roots, and lower germination by retarding biosynthesis and carbon metabolism.	[105,106]

Table 3. Cont.

Metal	Max. Permissible Limit (mg/L)	Concentration (mg/L)	Impact	References
As	0.01	0.002–73.6	Deposition of arsenic sulfide (orpiment) occurs at low temperatures (>120 °C) and low pH values in binary geothermal power plants, causing a reduction in heat transfer and blocking heat exchanger tubes. Arsenic may also interact with silica in a geothermal fluid to form metal–silica complex deposits.	[107,108]
			Irrigation with As-rich geothermal water disturbs the normal functioning of plant metabolism by reducing biomass accumulation, consequently inhibiting the plant's growth and compromising its reproductive capacity.	[109]
			Chronic exposure to arsenic in contaminated geothermal pools (balneotherapy) causes hyperpigmentation and increases the risk of skin cancer.	[110]
Hg	0.006	0.192–0.005	Under mildly reducing conditions, mercury co-precipitates as a mercury sulfide due to arsenic sulfide precipitation in geothermal power plants.	[103]
			Mercury is discharged as Hg ⁰ gaseous species through the cooling towers, harming wildlife and ecosystems.	[111,112]
			The biological formation of highly toxic methyl mercury in the sediments and water may lead to water body contamination and mercury accumulation in plants, marine fish, and shellfish.	[113,114]
Cd	0.003	0.005–1.63	In geothermal wells, cadmium co-precipitates with calcium carbonate and zinc sulfide, causing a reduction in the well capacity.	[115]
			Cd is relatively mobile in the aquatic environment compared to other trace metals. As a result, it seriously damages aquatic organisms' growth, reproduction, endocrine and immune systems.	[116]
			Plants growing on soil contaminated with Cd suffer reduced transpiration, inhibited growth, limited seed germination, chlorosis of leaves, and deformations of the root system, especially during the early growth stages. Cd also disrupts physiological functions, destroys the cellular membranes of soil microorganisms, and inhibits the enzymatic activity of soil.	[117,118]
Cr	0.05 *	0.012–1.033	Chromium tends to be strongly adsorbed onto organic and inorganic deposits in geothermal power plants.	[115]
			In soil, Cr (VI) can inhibit plant growth by reducing photosynthesis, producing reactive oxygen species (ROS), damaging root cells, affecting transpiration and nitrogen assimilation, and inhibiting trigger lipid peroxidation in plants.	[119,120]
			Swimming in Cr-rich geothermal water may cause irritant and allergic contact dermatitis. The symptoms of chromium allergic dermatitis include dryness, fissuring, erythema, swelling, and papules.	[105]

Table 3. Cont.

Metal	Max. Permissible Limit (mg/L)	Concentration (mg/L)	Impact	References
Cu	2.00	0.45–6.27	<p>An electrochemical corrosion reaction between copper ions in geothermal fluid and the iron of the carbon steel pipes may lead to massive precipitation of native copper in the geothermal pipeline system. At high copper concentrations, copper sulfide precipitation may also occur. In addition, it is able to incorporate other scale types, such as silica.</p> <p>Cu is an essential plant micronutrient for the growth and development of plants. However, excess Cu (20–100 mg/kg) harms soil microorganisms and plant growth and productivity.</p>	[103,121] [122,123]
Zn	5.00	0.228–250	<p>Zinc sulfide is one of the primary heavy metal scales in geothermal facilities. However, the precipitation of other zinc minerals from geothermal brine has also been identified, such as zinc carbonate and zinc chloride. In addition, Zn^{2+} can form a complex with organic and amorphous silica deposits.</p>	[124,125]

* Total concentration of trivalent chromium (III) and hexavalent chromium (VI).



Figure 2. The primary uses of geothermal fluids.

4.4. Fracking

Hydraulic fracturing, commonly known as fracking, is adopted to exploit crude oil, natural gas, shale gas and tight gas reservoirs for continued fossil fuel power generation. Fracking is an extraction process that involves injecting a large quantity of water mixed with chemicals. It operates at high pressures of up to 30 MPa to shatter rock formations and enhance gas recovery, as illustrated in Figure 3 [126]. The fracking fluid typically includes magnesium chloride as a stabilizing agent, polyethene glycol-1-octylphenyl ether as a friction reducer, sodium bromates as a breaker, 2-butoxyethanol as an active solvent, and glycol ether as a surfactant [127].

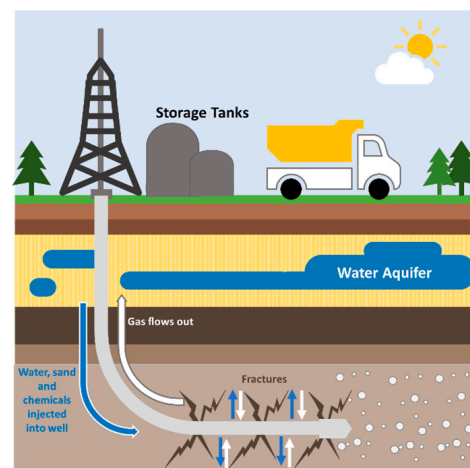


Figure 3. Diagram representing the process of fracking, adapted from [128,129].

The same method is used to stimulate geothermal reservoirs and improve the permeability of rocks. In fracking, a liquid mixture is injected at high pressure into the borehole. This liquid induces cracks in the formation of rock through penetrating perforations in the stones in the horizontal borehole. Once the pressure is released, a mixture of fracking fluid and formation water known as flowback water is withdrawn, which varies in composition from the initially injected fracking mixture. The flowback water is either sent to a wastewater treatment plant or deep-injection disposal [130]. When a well is not properly sealed or is damaged, fracking fluid or backflow water may contaminate groundwater with heavy metals, salts, and other chemicals [127]. A significant concern with respect to the fracking process is soil and groundwater contamination with fracking chemicals or flowback water components [131]. The formation water associated with the flowback water contains a variety of heavy metals, including lead, cobalt, arsenic, cadmium, chromium, zinc, copper, and nickel. Table 4 shows the concentrations of heavy metals in flowback waters from different drilling sites.

Table 4. The concentrations of the heavy metals in flowback from different drilling sites against the requirements for groundwater (GW).

Element	Concentration Range (µg/L)				GW * (µg/L)
	Gordalla, Ewers, and Frimmel [127]	Sun et al. [132]	Olsson et al. [133]	Knapik et al. [134]	
Lead	25–135	0.5–970	300–55,000	5–875	7
Arsenic	0.5–175	1–1100		50–210	10
Antimony	5–575	1–200			5
Cadmium	5–25	0.19–100		9–51	0.5
Chromium **	10–115	0.8–2200	300	10–13	7
Cobalt	10–50	2.9–169		10–102	8
Copper	10–56	6.5–18,000		<399	14
Mercury	6–730	0–65		10–305	0.2
Nickel	5–50	50–3200	1000		14
Zinc	25–9700	2.5–247,000	1200–290,000	200–20,480	58
Molybdenum	10–90	6.8–1980			35
Selenium	<5	2.5–350			7

* Insignificance thresholds for local and limited groundwater contaminations [135]; ** total concentration of trivalent chromium (III) and hexavalent chromium (VI).

5. Mechanisms for Removal

The mechanism for removing inorganic and organic pollutants depends on the nature of the contaminants and the chemical properties of the adsorbent surface [136]. Furthermore, there are co-existing carbonized and non-carbonized fractions with various removal mechanisms, as the biochar surface is heterogeneous. The mechanisms for the interaction of biochar with organic or inorganic pollutants include physical adsorption, precipitation, complexation, hydrophobic interaction [137], electrostatic interaction [138], pore-filling partition [139,140] and hydrogen bonding or π - π interactions, as illustrated in Figure 4. Heavy metals are immobilized on biochar surfaces through various mechanisms, with functional groups aiding the binding of polar molecules. The effectiveness of biochar for pollutant removal is influenced by its physico-chemical properties and factors like temperature, flow rate, pH, and contact time.

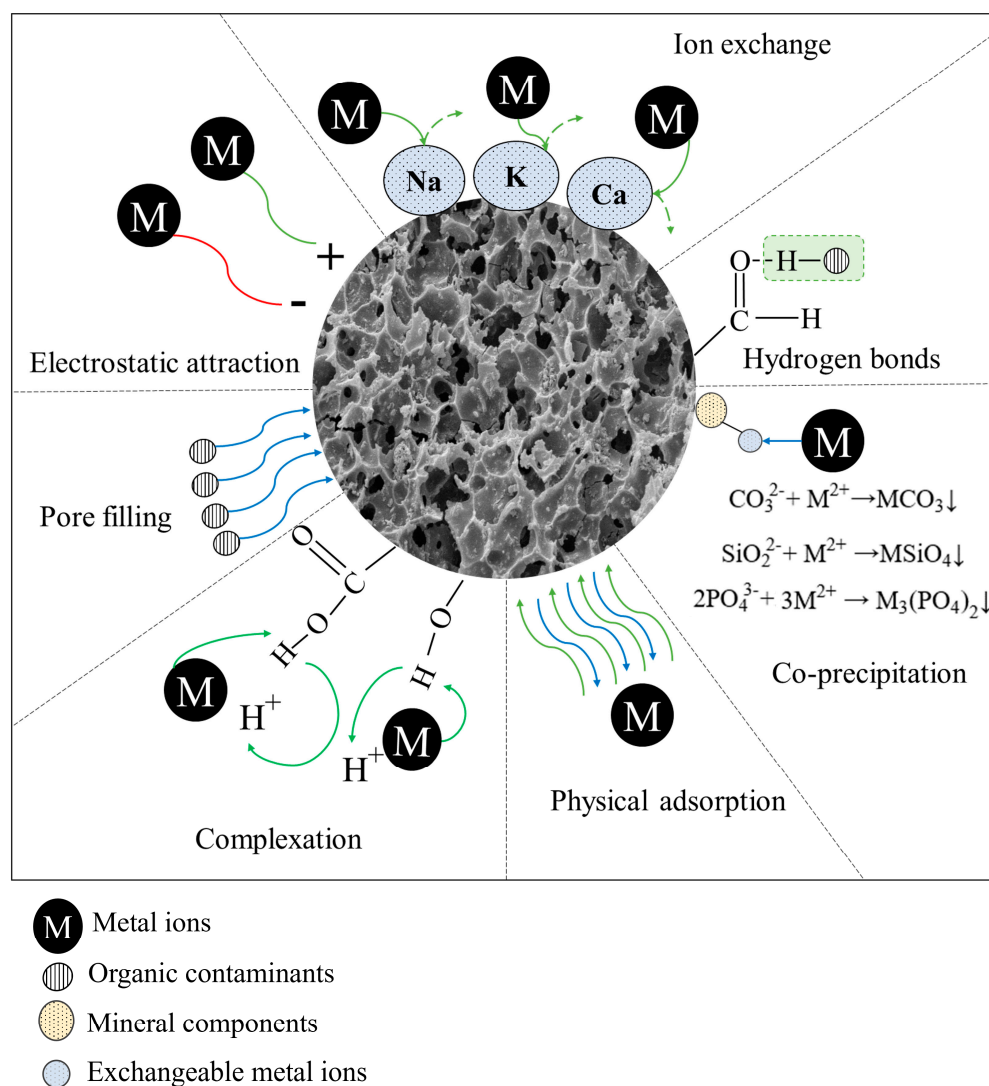


Figure 4. The mechanism for the pollutant adsorption onto biochar adapted from [141], biochar image adapted from [142].

Metal ions diffuse through the pores of the sorbent during the physical process, which results in the formation of chemical bonds [143]. The pore volume and surface area of biochar are favored by an increased carbonization temperature [144]. The likelihood of heavy metal ions adhering to the biochar surface or diffusing into micro-/mesopores has been found to increase with decreasing metal ion size [145,146].

Another mechanism for heavy metal remediation is ion exchange [147]. The ion exchange of metals with biochar happens when positively charged ions, such as H^+ [148], Fe^{2+} [149], K^+ [150], Ca^{+2} , Mg^{+2} , and Na^+ [151], from the surface of biochar are replaced with the target metal ions [144]. In one piece of work, the adsorption mechanism involving cations (Cu^{2+} , Ag^+) and biochar in an aqueous solution was examined, revealing a decrease in the solution's pH throughout the process. This observation solidified the evidence for the occurrence of ion exchange between the acidic functional groups present in the biochar, and the ions from the other species in the solution during the reaction [148]. The size of the metal ions and biochar surface functional groups are key factors in ion exchange, but biochar's cation-exchange capacity has been seen to decrease at pyrolysis temperatures above 350 °C [143]. Additionally, the sorbents altered the water chemistry by introducing base cations like Ca^{+2} , Mg^{+2} , K^+ , and Na^+ . There was an increase in the release of base cations in the presence of metals, suggesting surface cation exchange on the biochar. Particularly, wood ash treatments exhibited higher base cation release, indicating the role of cation exchange in immobilization. While ion exchange is a significant mechanism for immobilizing Pb, Cu, Zn, and Cd according to various studies, precipitation remains the primary process [151]. In their investigation on the adsorptive mechanisms of sludge biochar on Cr (III) and Cr (VI), Chen et al. discovered that the adsorption capacity of the sludge biochar on Cr (III) was higher, primarily due to ion exchange between Cr (III) and the Ca (II) and Mg(II) ions in the ash components of the biochar matrix [152].

Electrostatic attraction between the negatively charged surface of biochar and positively charged heavy metal ions is a key mechanism that enhances biochar's adsorption capacity for water treatment [153]. Parameters such as pH, ionic radius, metal valence, and zeta potential influence the strength of these interactions [154]. Zhang et al. reported that metal and heteroatom co-doped biochar composites (MHBCs) can adsorb Cr (VI) and catalyze its reduction to Cr (III), with Fe_2O_3 particles and nitrogen hybrids playing a key role. These interactions are facilitated by the positively charged nitrogen groups ($-N=+$) on the surface, which attract Cr (VI), and its subsequent reduction is driven by nZVI and $-NH$ -groups. At pH 2, protonation enhances the electrostatic attraction of Cr (VI) [155,156].

Qui et al. compared biochars from rice and wheat straw with commercial activated carbon (AC), finding that the biochars adsorbed Pb (II) more effectively, particularly at higher pH levels. This enhanced performance is attributed to electrostatic interactions between the positively charged Pb (II) and negatively charged functional groups on the biochar surfaces. The deprotonation of these functional groups, as shown by MINTEQA2 calculations, increases the adsorption efficiency as the pH rises [157].

Qian et al. prepared rice straw biochar at various pyrolysis temperatures and oxidized it with HNO_3/H_2SO_4 to introduce oxygenated groups. These groups, particularly the carboxylic ones, facilitated Cd adsorption at acidic pH levels (2.0–3.5) via electrostatic interactions [158]. Manganese- or alkali-modified biochars demonstrated higher affinity for Cd(II) compared to iron-modified ones, as the basic surface of manganese-modified biochar enhances electrostatic attraction with cations, whereas the acidic nature of iron oxide biochar limits this due to the high surface proton content [159].

The porous structure of biochar allows pollutant adsorption via the pore-filling mechanism, especially at low solute concentrations [160,161]. This process is particularly relevant for organic compound adsorption, although it also applies to fluid remediation [162], as shown in Figure 4. Zhang et al. produced biochar from sycamore flock, activated with K_2CO_3 , for the removal of oxytetracycline hydrochloride (OTC-HCl), where hydrogen bonding, electrostatic interactions, and electron donor–acceptor (EDA) interactions contributed to the adsorption, with pore filling as the dominant mechanism [163]. Sun et al.

employed biochar from animal and poultry manure, produced via hydrothermal methods, to adsorb bisphenol A, 17 α -ethinyl estradiol, and phenanthrene, with pore filling identified as the primary adsorption mechanism [164].

Another mechanism for the adsorption of polar organic molecules on biochars is hydrogen bonding. The abundance of polar groups on biochar improves the H-bonding between biochar and counter ions that contain electronegative components, which facilitate water treatment [165]. The mechanism used by Ni et al. to study the adsorption of the allelopathic aromatic acids, cinnamic and coumaric onto various biochars was hydrogen bonding [166]. Dibutyl phthalate (DBT) adsorption by biochars made from rice straw and swine dung, for instance, was ascribed to H-bonding between H-donor groups or water molecules on the biochar and O-atoms on the DBT ester group [167].

The immobilization of inorganic pollutants by biochar is also attributed to precipitation, enabled by biochar's elevated pH and metal content [168]. During pyrolysis, the decomposition of cellulose and hemicellulose generates organic acids, lowering the pH, but as temperatures exceed 300 °C, alkali salts are released, increasing the pH to above 10, stabilizing between 350 and 500 °C due to the removal of alkali salts [169]. Chen et al. demonstrated that biochar composites with hydroxyapatite/calcium silicate hydrate precipitate heavy metals (Cu, Cd, Pb and Zn) by reacting with phosphate ions [170]. Li et al. found orthophosphate effective in precipitating Cu (II) from contaminated soil using struvite (NH₄MgPO₄·6H₂O)-biochar composites, forming Cu (II) phosphate solids at pH 5–7 [168].

Inyang et al. showed that sugarcane bagasse biochar, especially from anaerobically digested bagasse (DBC), removes Pb via precipitation, forming (Pb₃(CO₃)₂(OH)₂) and cerussite (PbCO₃), confirmed by XRD and SEM [171]. Similarly, wheat straw biochar loaded with nano-FeS removed Cr (VI) from soil through the reduction and precipitation of Cr₂O₃, Fe₂O₃, and Fe(OH)₃. Su et al. used MgAl-layered double hydroxide (MgAl-LDH) loaded on biochar to remove Pb (II) and Cu (II). XRD and XPS revealed the formation of Pb₃(CO₃)₂(OH)₂ and Cu(OH)₂ on the biochar surface, confirming precipitation as a key removal mechanism [172].

During complexation, multi-atom structures are created, characterized by distinct metal–ligand interactions [173]. This process involves the interaction of the d-orbitals of heavy metals with oxygen-containing functionalities. Consequently, augmenting the abundance of oxygen-containing functional groups on the biochar surface can lead to an enhancement in the efficiency of heavy metal removal through complexation [144]. The oxygen content on the biochar surface has been observed to rise gradually with time, possibly attributed to surface oxidation and the formation of carboxyl groups. Consequently, it is plausible that metal complexation could also increase over time [174]. In a study conducted by Liu et al., rice husk and wood biochars underwent modification with calcium silicate (CaSiO₃) using a ball milling method, which was then employed for Cd removal from water. Fourier-transform infrared spectroscopy (FTIR) analysis showed weakened –COO– peaks and the near disappearance of –OH groups on the biochar after Cd (II) adsorption, indicating complexation with oxygen-containing functional groups [175]. Mishra et al. investigated the adsorption behavior of U (VI) on eucalyptus biochar. The subsequent XPS analysis validated that the primary mode of uranium adsorption onto the biochar surface occurred through complexation interactions between the surface functional groups and U (VI) species [176].

5.1. Kinetics

The kinetic study of metal removal from water using biochar offers insight into the potential adsorption processes and reaction pathways [177]. Understanding the reaction pathways, the mechanism of biosorption (referring to the process wherein heavy metals are removed from an aqueous solution through their passive binding to non-living biomass), and the kinetics requires the investigation of the kinetic model for biosorption studies. It aids in choosing the biosorption process's physiochemical interactions, mass transfer, and

rate-determining phases [178,179]. To explain the adsorption phenomenon, many kinetic models, including first-order, pseudo-first-order, second-order, pseudo-second-order, and Elovich models, have been tested [178].

In 1989, the pseudo-first-order (PFO) reaction was proposed for the adsorption of oxalic acid and malonic acid onto charcoal [180]. The pseudo-first-order model operates on the assumption that the rate at which the solute adsorbs is directly proportional to the disparity between the saturated concentration and the amount of adsorptive material adsorbed over time [11]. The equation for the pseudo-first-order model is shown in Equation (1), where the rate constant (k_1) is a function of the process conditions. According to certain studies, the k_1 is either an increasing function of C_0 or not reliant on C_0 [181,182]. Conditions such as the pH and temperature exhibit an impact on the k_1 value, although it would be difficult to empirically isolate the influence of these two elements on a k_1 value because the equilibrium behavior is affected by both:

$$\ln(q_e - q_t) = \frac{k_1}{2 \times 303} t \quad (1)$$

The adsorption rate is assumed to be second-order in the pseudo-second-order (PSO) model relative to the accessible surface sites. The pseudo-second-order kinetic theory dictates that the adsorption rate is governed by interactions such as ion sharing and transfer between the adsorbent and adsorbate [11]. In contrast to the pseudo-first-order model, which assumes that the rate of occupation of adsorption sites is proportional to the number of unoccupied sites on the adsorbent, the pseudo-second-order model assumes that the rate of occupation of adsorption sites is proportional to the square of the number of unoccupied sites on the adsorbent.

The PSO model can simulate most environmental kinetic adsorption, proving its supremacy over other models. The constant k_2 , as depicted in Equation (2), is a timescale factor that decreases with increasing C_0 , much like the PFO model [183,184]. The most used models in the research on the kinetics of environmental adsorption are the PFO and PSO models. However, the PFO model is typically less well suited than the PSO model, which uses a least-square discrimination technique. For this model, the q_e (the amount of metal ions adsorbed at equilibrium (mg/g)) is remarkably further from the experimental value than that provided by the PSO model [185]:

$$\frac{t}{q_t} = \frac{1}{k_2 q_e^2} + \frac{t}{q_e} \quad (2)$$

When describing the adsorption of CO on manganese dioxide, Roginsky and Zeldovich first proposed the Elovich equation [180], the linear form of which is shown in Equation (3). When plotting q vs. $\ln t$, the kinetic observation of the Elovich equation should result in a straight line, where q is the initial adsorption rate, and β is the desorption constant associated with the amount of surface covering and activation energy for chemisorption. The slope is $1/\beta$, and the intercept is $[\ln(\alpha\beta)]/\beta$:

$$q_t = \frac{1}{\beta} \ln(\alpha\beta) + \frac{1}{\beta} \ln t \quad (3)$$

Table 5 shows the kinetic models, isotherm models, and removal mechanisms for heavy metal removal using non-functionalized biochars from recent studies.

Table 5. Heavy metal kinetics, adsorption isotherms, and removal mechanisms using biochars from recent studies.

Biomass	Method and Conditions	Pollutant	Reaction Conditions	Predominant Removal Mechanisms	Adsorption Capacity/Removal Rate	Adsorption Kinetic Model	Adsorption Isotherm Model	Reference
Rice husk	Pyrolysis, 500 °C, 2 h, N ₂ atmosphere	Cr (VI)	Initial concentration—100 mg/L; pH—3.0 ± 0.1; dose—5 g/L; temperature—25 ± 1 °C.	Electrostatic attraction	84.2%	Elovich model	Freundlich model	[186]
Red mud	Pyrolysis, 700 °C, 0.5 h, CO ₂	As (V)	Initial concentration—5.9 mg L ^{−1} ; pH—3.0–10.0; dose—1 g L ^{−1} .	Chemisorption	>77.6%	Pseudo-second-order model	Langmuir model	[187]
Myriophyllum aquaticum	Pyrolysis, 700 °C, 1 h, N ₂	Cr (VI)	Initial concentration—100 mg/L; dose—1 g/L; pH—2.	Electrostatic interactions and complexation	175.4 mg g ^{−1}	Pseudo-second-order model	Langmuir model	[188]
Pigeon waste	Pyrolysis, 600 °C, 2 h, N ₂	Cr (VI)	Initial concentration—80 mg/L; dose—1.5 g/L; pH—4.	Reduction and precipitation	94.12%	Pseudo-second-order model	Langmuir model	[189]
Tea waste	Pyrolysis, 700 °C, 2 h, N ₂	Cu (II)	-	Complexation and electrostatic interaction	-	Elovich model	Freundlich model	[190]
Peanut shell	Pyrolysis, 500 °C, N ₂	Pb (II)	Initial concentration—100 mg/L; pH—5.	Complexation and electrostatic interaction	97%	Quasi-second-order model	Langmuir model	[191]
Rice husk	Pyrolysis, 600 °C, 3 h, N ₂ flow	Pb (II)	Initial concentration—60 mg/L; pH—6; dose—0.07 g.	Complexation, cation exchange, and electrostatic attraction	122.3 mg g ^{−1}	Pseudo-second-order model	Langmuir model	[192]
Banana peel	Hydrothermal synthesis, 180 °C, 24 h	As (V)	Initial concentration—50 mg/L; pH—7; dose—7.51 mg g ^{−1} .	Metal ion exchange	96.7%	Pseudo-second-order model	Langmuir and Freundlich models	[193]
Banana peel	Hydrothermal synthesis, 180 °C, 24 h	Pb (II)	Initial concentration—50 mg/L; pH—7; dose—6.10 mg g ^{−1} .	Metal ion exchange	93.7%	Pseudo-second-order model	Langmuir and Freundlich models	[193]
Pomelo peels	Pyrolysis, 300–700 °C, 1 h	Sb (III)	Initial concentration—100 mg/L; dose—0.5 g/L.	Inner-sphere complexation, H-bonding, and electrostatic attraction	77.44 mg g ^{−1}	Pseudo-second-order model	Freundlich and Langmuir models	[194]

Table 5. Cont.

Biomass	Method and Conditions	Pollutant	Reaction Conditions	Predominant Removal Mechanisms	Adsorption Capacity/Removal Rate	Adsorption Kinetic Model	Adsorption Isotherm Model	Reference
Water caltrop shell	Pyrolysis, 850 °C, 1 h, N ₂	Cd (II)	Initial concentration—50 mg/L; dose—1.0 mg/L; pH—7.0.	Electrostatic attraction and π -bond coordination Electrostatic attractive, surface complexation, chemical precipitation, and reductive reaction	86.25 mg g ^{−1}	Pseudo-second-order model	Langmuir model	[195]
Peanut shell	Pyrolysis, N ₂ atmosphere	U(VI)	Initial concentration—100 mg/L; pH—4.16; dose—1 g/L.	Complexation and precipitation	92.45 mg g ^{−1}	Pseudo-second-order model	Freundlich equilibrium model	[196]
Red gram seed coat	Pyrolysis, 450–650 °C, 2 h, N ₂	Cu (II)	Initial concentration—350 ppm; dose—0.6 g/L; time—90 min.	Complexation	493.34 mg g ^{−1}	Pseudo-second-order model	Langmuir isotherm	[197]
Wheat straw	Microwave pyrolysis, power: 100–600 W, N ₂ gas (flow rate: 50 mL min ^{−1})	Pb (II)	pH—6; dose—0.5 g/L.	Complexation and precipitation	139.44 mg g ^{−1}	Pseudo-second-order model	Langmuir isotherm	[198]
Wheat straw	Microwave pyrolysis, power: 100–600 W, N ₂ gas (flow rate: 50 mL min ^{−1})	Cd (II)	pH—6; dose—0.5 g/L.	Complexation and precipitation	52.92 mg g ^{−1}	Pseudo-second-order model	Langmuir isotherm	[198]
Wheat straw	Microwave pyrolysis, power: 100–600 W, N ₂ (flow rate: 50 mL min ^{−1})	Cu (II)	pH—5; dose—0.5 g/L.	Complexation and precipitation	31.25 mg g ^{−1}	Pseudo-second-order model	Langmuir isotherm	[198]
Kenaf	Pyrolysis, 450 °C, 2 h	Cr (VI)	Initial concentration—50 mg/L, pH 2, dose—4 g/L	Electrostatic attraction and inner-pore mechanism	63.57 mg g ^{−1}	Pseudo-first-order model	Freundlich isotherm	[199]
Reed straw	Pyrolysis, 450 °C, 2 h, N ₂ atmosphere	Cr (VI)	Initial concentration—100 mg/L, pH 4.5, dose—2 g/L	Reduction, surface ion exchange	49.17 mg g ^{−1}	Pseudo-second-order model	Redlich–Peterson model	[200]

Table 5. Cont.

Biomass	Method and Conditions	Pollutant	Reaction Conditions	Predominant Removal Mechanisms	Adsorption Capacity/Removal Rate	Adsorption Kinetic Model	Adsorption Isotherm Model	Reference
Loofah sponges	Pyrolysis, 700 °C, 2 h, N ₂ atmosphere	Cr (VI)	Initial concentration—40 mg/L, pH 3, dose—0.5 g/L	Physical adsorption and precipitation, surface complexation, and ion exchange	30.14 mg g ^{−1}	Pseudo-second-order model	Freundlich isotherm	[201]
Loofah sponges	Pyrolysis, 700 °C, 2 h, N ₂ atmosphere	Cu (II)	Initial concentration—40 mg/L, pH 3, dose—0.5 g/L	Physical adsorption and precipitation, surface complexation, and ion exchange	54.68 mg g ^{−1}	Pseudo-second-order model	Freundlich isotherm	[201]
Rape stalk	Microwave pyrolysis, 400–600 °C, N ₂ atmosphere	Cd (II)	Dose—1 g/L, pH 5	π–electron interaction	53.17 mg g ^{−1}	Pseudo-second-order model	Langmuir isotherm	[202]
Douglas fir green wood chips	Pyrolysis, 700 °C, 1 h, N ₂ atmosphere	Pb (II)	Initial concentration—5–1000 mg/L, temperature—318 K, pH 5	Ion exchange	140 mg g ^{−1}	Pseudo-second-order model	Langmuir isotherm	[203]
Douglas fir green wood chips	Pyrolysis, 700 °C, 1 h, N ₂ atmosphere	Cd (II)	Initial concentration: 5–1000 mg/L, temperature—318 K, pH 6	Ion exchange	29 mg g ^{−1}	Pseudo-second-order model	Langmuir isotherm	[203]
Douglas fir green wood chips	Pyrolysis, 700 °C, 1 h, N ₂ atmosphere	Cr (VI)	Initial concentration: 5–300 mg/L, temperature—318 K, pH 2	Electrostatic interactions	127.2 mg g ^{−1}	Pseudo-second-order model	Freundlich isotherm	[203]

5.2. Influence of Parameters on Removal Process (pH, Temperature, Flow Rate)

Numerous factors such as pH, flow rate and temperature, can influence the removal performance capacities of different adsorbents. The pH can cause protonation or deprotonation and the charging of the surface functional groups of biochar, resulting in varied adsorption capacities for removing pollutants [204,205]. As the pH of the aqueous solution rises, functional group deprotonation happens and, consequently, the adsorption capacity escalates towards cationic metals. However, electrostatic repulsion between protons and metal ions in aqueous media increases if the solution pH decreases. Thus, the adsorption capacity decreases due to the competition between cations for the adsorption sites [204].

For example, investigations by Gao et al. monitored cadmium adsorption using CaCl_2 modified biochar from selenium-rich straw. The authors examined a range of pH values (2–7) for the adsorption of Cd (II) onto their biochar, reporting that the optimum pH for the highest removal was pH 5. However, if the pH level of the simulated wastewater solution containing Cd increased over 5, the overall effect on the adsorption was considered negligible [206], whereas Yan et al. used cornstalk biochar for the adsorption of Pb (II) and Cd (II), reporting that as the pH of the solution increases, the adsorption performance improves. Since there are many positive ions present in the solution at lower pH levels, electrostatic repulsion becomes highly significant. Electrostatic attraction increasingly replaces electrostatic repulsion when the pH rises, leading to a rise in the adsorption capacity [207]. Sakhiya et al. reported that with a rise in pH from 3 to 6, the adsorption capacity for Pb (II) and Zn (II) moderately increased. Most of the functional groups available on the biochar surface become protonated and positively charged at low pH values. In solution, the presence of H^+ and H_3O^+ ions hinder the cation adsorption sites on biochar. Therefore, the electrostatic repugnance between the positively charged biochar surface and metal ions results in a lower sorption rate at low pH [208].

The work conducted by Li et al. synthesized activated carbon (EPAC) derived from *Enteromorpha prolifera* (EP) through zinc chloride activation. The adsorption capacity exhibited a notable increase, ascending from 75.52 to 91.54 mg/g at a Pb (II) ion equilibrium concentration of 10 mg/L as the temperature was increased from 5 to 35 °C. These findings suggest that the adsorption process of Pb (II) ions onto EPAC is characterized by endothermic behavior. In other words, elevating the temperature facilitates a higher diffusion rate of Pb(II) ions, amplifying the number of adsorption sites and consequently augmenting the adsorption efficacy of the EPAC [209]. Similarly, in a study completed by Yan et al., biochar derived from cornstalks was prepared and evaluated for its ability to adsorb Pb (II) as well as Cd (II). The research revealed minimal variation in the adsorption capacity at different temperatures. Specifically, while the Pb adsorption exhibited an increasing trend, the same trend was not observed for Cd. This increasing trend implies that higher temperatures supplied adequate energy for heavy metals to overcome the diffused double layer (an ionic structure that defines the disparity of the electric potential near a charged surface), thereby facilitating their adsorption onto the interior structure of the biochar [207].

Hakeem et al. considered the effect of temperature on the adsorption of various heavy metals, it was found that for Na, K, Mg, and Zn, the temperature had little influence on the extraction, whereas for Cu, Cd and Ni, the temperature had a significant role. It was reported that for Ni and Cd the ideal extraction temperature was 100 °C, removing 76% and 99%, respectively, whereas for Cu, it was found that 85% could be removed at 63 °C. At all temperatures tested (25 °C, 63 °C and 100 °C), the impact of extraction was more pronounced for Ni than for Cu and Cd. For instance, the Ni extraction at 100 °C reached 50% in 20 min, whereas the same extraction at 25 °C took ~180 min. The marginal increase in Cd extraction (10% to 15%) was identical up to the first 60 min across all temperatures. After that point, the extraction rate for the 25 °C experiment continued to increase, whereas for 100 °C, it fell significantly, and the extraction converged at 80% at 180 min. In the investigation, as the temperature rose from 25 to 63 °C, the amount of Cu extracted increased from 73% to 85%. However, a further rise in temperature to 100 °C reduced the amount of copper extracted to 35% [210]. By modifying the solubility and

intermolecular interaction, the temperature influences the rate of adsorption [154]. This being said, Bongosia et al. demonstrated how a structured mesoporous biochar derived from bagasse waste could be used at a high pH (pH 10) to rapid effect for Cu removal at room temperature, outperforming many other biochars which favor low pH values (reaching 97.85% removal in 5 min). This alternative operational environment enables the produced biochars to be applicable to carbonate-rich mine waters and ancestral landfill sites, which are known to be basic by nature [142].

Laboratory-scale, continuous-system biosorption research is crucial for designing the biosorption process for industrial use. Both wastewater treatment applications and increasing the effectiveness of the biosorbent depend on the employment of packed-bed columns. Another crucial factor that has a big impact on continuous treatment systems is the flow rate, otherwise known as the adsorbent residence time. The adsorption of several contaminants, including metals, phosphates, and carbofuran by biochar produced from a variety of biomass feedstocks has been shown to have an inverse relationship between the flow rate and adsorption capacity [136].

Hammo et al. utilized capsicum annum seeds to create biochar (CASB), and the impact of the flow rate on Pb (II) biosorption was tested at different flow rates (0.5, 1.0, 2.0, 4.0, and 6.0 mL min⁻¹). It was deduced that when the solution flow rate escalated from 1.0 to 2.0 mL min⁻¹, there was a drop in the biosorption yield of the CASB from 51.75 ± 1.68% to 34.63 ± 0.89%, and after that, it reached a plateau, demonstrating equilibrium [136,142]. In another investigation by Aran et al., the efficacy of various biochar types (obtained from chicken manure, eucalyptus, corncob, olive mill, and pine sawdust) for the removal of copper from aqueous solutions was examined using a continuous-flow system. The study focused on analyzing the breakthrough time (t_b) and saturation time (t_e) in relation to different flow rates. Results indicated an inverse linear relationship between the flow rate and both the t_b and t_e within the range of 2.5–7.0 mL min⁻¹. However, a lesser degree of variation was observed in these parameters within the range of 7.0–13.0 mL min⁻¹. This phenomenon can be elucidated by considering that beyond a certain threshold flow rate, the residence time of the solution within the column decreases, impeding sufficient interaction with the biochar surface and thereby causing the premature appearance of the solute in the effluent before reaching the adsorption equilibrium [211].

In a study conducted by Asadullah, the authors transformed hydrochar (HC) derived from hydrothermally synthesized *Lepironia articulata* (LA) into biochar (LABC) using KOH. Additionally, natural bentonite clay was modified with a cationic surfactant called bencylhexadecyldimethyl ammonium chloride (BCDMACl). The two adsorbents, LABC and modified bentonite (MB), were combined to create a monolith (LABC-MBm) using two different binders: polyvinylidene difluoride (PVDF) and methylcellulose (MC). The study investigated the impact of flow rate on the adsorption of heavy metals. The flow rate of heavy metals was adjusted between 5 and 15 mL/min, while keeping the bed height and initial concentration constant at 4 cm and 100 mg/L, respectively. As the flow rate increased from 5 to 15 mL/min, the breakthrough time (t_b) decreased from 80 to 35 min. At lower flow rates, breakthrough occurred sooner because the heavy metals had more time to interact with the adsorbent bed, resulting in lower concentrations of heavy metals in the effluent. The total amounts of heavy metals adsorbed (q_{tot}) at a flow rate of 5.0 mL/min and a bed depth of 4 cm were determined to be 72.5 mg for Ni²⁺, 68.2 mg for Zn²⁺, and 78.5 mg for Cr³⁺. Additionally, the breakthrough capacities were found to be 11.22 mg/g for Ni²⁺, 10.4 mg/g for Zn²⁺, and 15.58 mg/g for Cr²⁺. These values were higher than the adsorption capacities achieved using only LABC and MB [212].

5.3. Recyclability—Regeneration

The regeneration of adsorbents involves the following two principles: adsorbate desorption and adsorbate decomposition/restructuring [213]. Instead of “burning it and dumping it” in the environment, continuing the single-use economy, biochars can be regenerated for reuse. From an economic perspective, the biosorbent’s suitability for

the regeneration process is crucial since it enables the biosorbent to be used in several cycles [214].

Various technologies, such as thermal regeneration, solvent/acid regeneration, microwave irradiation regeneration, and supercritical fluid regeneration, can be used to regenerate biochar [142]. Thermal regeneration stands out as one of the most potent techniques for achieving desorption. Here, the adsorbate undergoes carbonization and decomposition under high temperatures. Eventually it transforms into molecules smaller than the pore size of biochar, facilitating their release [215].

In a study conducted by Greiner et al., pine biochar produced at 850 °C was exposed to background dissolved organic matter derived from surface water (~4.2 mg/L, UV absorbance at 254 nm (UVA254)) and sulfamethoxazole (SMX) in a column setup. Following exposure, the biochar was subjected to a semi-oxic thermal regeneration process at 600 °C. Comparing the exhausted biochar to its fresh counterpart, the heat-treated biochar exhibited approximately 3.5 times and 3 times higher adsorption capacities for SMX and UVA254, respectively. Similar improvements in the adsorption capacity were observed when the heat treatment was applied to fresh biochar. Interestingly, after a second exhaustion–regeneration cycle, both the adsorption capacity and the BET surface area continued to increase, although the adsorption efficiency remained constant due to mass loss [216]. A negative effect of this method is the elevated energy usage during thermal regeneration, reaching temperatures as high as 800 °C, which amplifies production expenses. This energy consumption might constitute as much as 50% of the overall production cost for a new biochar [217].

Another approach involves employing a chemical regeneration process utilizing solvents (solvent regeneration). This method has seen widespread use in regenerating biochar, enhancing its reusability, and resulting in substantial reductions in operating costs. By adjusting the temperature and pH of the solvent, solvent regeneration breaks the adsorption equilibrium. This is achieved by utilizing the equilibrium relationship between the biochar, solvent and adsorbate [215]. Different acids, bases and organic solvents are used as reagents for desorption.

Researchers explored the regeneration of magnetic biochar made from eucalyptus leaves for Pb (II) removal. The biochar was incorporated with ferrous oxides to assess the regeneration's impact on iron loss and magnetic properties. Four regenerative agents—0.1 mol/L HCl, acetic acid, EDTA-2Na, and deionized water—were tested. EDTA-2Na proved the most effective, achieving an 84.1% desorption efficiency while minimizing the iron loss, thus preserving the biochar's magnetic properties. Additionally, the surface area and pore volume of the biochar increased across regeneration cycles, likely due to ash breakdown and iron oxide release [218].

Jia et al. used a MgFe-layered double hydroxide magnetic biochar (LMBC) for Pb (II) removal from an aqueous solution. Regeneration with 2 M NaOH for 1.5 h over five cycles showed an initial 83% removal efficiency, decreasing to 76.5% by the fifth cycle. The Pb(II) desorption was attributed to surface co-precipitation ($\text{Pb}_3(\text{CO}_3)_2(\text{OH})_2$) and NaOH, while the chemical structure of the LMBC remained unaffected [219].

A third investigation developed a novel three-dimensional MnO_2 -modified biochar-based porous hydrogel (MBCG) for Cd (II) and Pb (II) removal. Regeneration involved 0.3 M HNO_3 and 0.03 M NaOH treatments, retaining the hydrogel's structure and performance over five cycles. After regeneration, the MBCG maintained adsorption capacities of 15.55 mg g^{−1} for Cd(II) and 34.21 mg g^{−1} for Pb(II), preserving 92.1% and 80.5%, respectively, of the initial adsorption capacities observed with fresh MBCG [220].

Adsorbents can be regenerated using microwaves in two main ways. The first method is to directly heat adsorbents that contain pollutants. The procedure involves the heat degradation of the pollutant molecules attached to the adsorbent's surface. The second method is microwave-assisted solvent desorption, in which the adsorbent is dissolved in a solution and microwave radiation is applied to facilitate the pollutant removal [221]. For instance, through microwave heating in a CO_2 atmosphere, Oladejo et al. successfully

regenerated spent activated carbon from a wastewater treatment facility. It was found that microwave-assisted regeneration can restore ~83% and ~90% of the adsorption capabilities when compared to freshly made activated carbon [222].

Supercritical fluid is another regeneration method that can remove pollutants from biochar. It is possible to use supercritical fluid, such as CO₂, as an extractant by adjusting the operating pressure. Supercritical fluid regeneration has the advantages of rapid working cycles, low operating temperatures, and less biochar loss [223]. However, this approach is still in the experimental stage (a low technology readiness level) and is not yet cost-effective for large-scale applications.

Using microorganisms to remove adsorbates is a cost-effective method and is an ecologically benign process known as biological regeneration [224]. In the work of Liao and colleagues, it was discovered that microorganisms broke down the organic matter that the biochar had adsorbed, allowing the biochar to undergo biological regeneration. This process helped maintain the biochar's long-term adsorption capacity, with a regeneration rate of 75% observed both before and after the resting period [224].

6. Biochar Functionalization

The physicochemical properties of biochar such as the surface area, pore volume, pore diameter, and surface functional groups, have a direct impact on how it will perform for both CDR and the adsorption of heavy metals [225]. By modifying the surface properties of the biochar through different pre-/post-treatment methods and functionalization, it is possible to design more efficient biochar-derived materials to enhance water treatment [226].

6.1. Hybrid Biochars and Membranes

In recent years, modifications of biomass-derived biochar with the addition of a chitosan biopolymer have generated flourishing interest. It has been well acknowledged in the literature that the addition of chitosan to biochar greatly improves the physicochemical properties, enriching the surface functional groups and surface area [227,228]. One piece of work designed a novel hybrid bio-adsorbent derived from biochar and chitosan for heavy metal removal in industrial and domestic effluents [229]. The study investigated the effect of different compositions of biochar-modified chitosan membranes on the sorption characteristics of different heavy metals, including Cu, Pb, As and Cd. From the Langmuir adsorption model fitting results, the chitosan-modified bio-adsorbent was found to be a highly effective, low-cost absorbent with high rates of heavy metal uptake, specifically for Cu and Pb [229]. However, despite the enhanced adsorption capacity of the chitosan-modified biochar, the downstream recovery of the solid particles from treated water often requires post-treatment steps such as sedimentation, centrifugation, and filtration, which imposes additional operating costs. Therefore, the recovery issue of biochar-based adsorbents has been further addressed by introducing and impregnating magnetic properties into the biochar-based adsorbent. Recently, Chin et al. reviewed the feasibility of different chitosan-modified magnetic biochars for heavy metal removal from aqueous solutions [4], and this, along with numerous studies, demonstrated not only the superior heavy metal removal performance of chitosan-modified biochar but also the efficient separation/recovery of the adsorbent in post-treatment processing.

Ainscough et al. developed a novel hybrid ceramic membrane and functionalized it with epoxidized carbon nanotube materials [230]. The membrane was not only capable of maintaining its flux over 10 days, even when tested with used motor oil, but it was also able to remove heavy metals, including Cd, Hg, Ni, Co and Pb, to a very high degree of 99.3%. The spent membrane was cleaned easily with a 50:50 acetic acid:water solution and regenerated to almost the complete adsorptive capacity. The same research team tested the same membrane with contaminated river water from Rio Las Vacas in Guatemala City, and the results demonstrated that the hybrid superhydrophilic ceramic membrane possesses an excellent microbial removal performance and presented antifouling properties, since the

test used an oil–water emulsion. Sri et al. investigated the removal of cadmium (Cd^{2+}) and lead (Pb^{2+}) in water by using a hybrid adsorption process. This accommodated natural zeolites found in the Aceh province of Indonesia as adsorbents, followed by ultrafiltration membrane filtration [231]. It was found that the hybrid adsorption and ultrafiltration process were capable of achieving maximum Cd^{2+} and Pb^{2+} removal rates of 86% and 89%, respectively.

In another study by Cermikli and co-workers, the team utilized an N-methyl-D-glucamine (NMD) membrane and functionalized it with three types of novel ion-exchange resins: revealing gel (1JW), expanded gel (2JW), and epidermal-like structure (2PTN), prior to applying it for boron and arsenic removal from saline geothermal waters simultaneously [232]. From the results, the NMD membranes functionalized with 2JW offered the highest boron removal performance of 92%, whereas the maximum arsenic removal was found to be 35.8% by the 1JW resin. Both novel resins were found to outperform the commercial Dowex XUS 43594.00 resin in terms of the boron and arsenic removal performance.

6.2. Biochar-Based Composites

Nanobiochars are a type of biochar with a particle size less than 100 nm, providing improved surface, chemical and physical properties [233]. As a potential alternative to biochar for waste management, nanobiochars exhibit superior adsorption of pollutants, nutrients, and toxins in soil systems [234]. Biochar nanocomposites can be further upgraded through the combination of benefits from the nanomaterials, with the availability of several functional groups, such as hydroxyl ($-\text{OH}$), carboxyl ($-\text{COOH}$), and amine ($-\text{NH}_2$) groups. These functional groups are crucial to the use of biochar, especially for water purification [148].

Xiao et al. discovered micro- and nano-engineered nitrogenous (nitrogen-functionalized) biochars, derived from cow bone meal and pyrolyzed at various temperatures, which were effectively engineered using ball milling. These engineered materials were then employed for the removal of heavy metals like Cu (II), Cd (II), and Pb (II) from aqueous solutions. Among the ball-milled bone biochar samples, the biochar synthesized at 600 °C exhibited a superior adsorption performance, attributed to its micro-/nanoscale size and extensive surface area achieved through ball milling and pyrolysis [235]. Work completed by Yu and co-workers used a facile ball-milling method to fabricate a novel ZnO/biochar nanocomposite. The homogeneous distribution of ZnO nanoparticles on the biochar skeleton improved the nanocomposite's methylene blue adsorption capacities while also giving it photocatalytic capability [235,236].

Zhang et al. created a highly porous nanocomposite material with a high capacity for ionic pollutant adsorption made of MgO nanoflakes in a charcoal matrix. Each MgO–biochar nanocomposite demonstrated outstanding removal efficiencies for phosphate and nitrate in aqueous solution [237]. Hosny and his colleagues designed a novel, inexpensive, and reliable path for the phytofabrication of a nanocomposite Ag–Cu biochar. It was found that the nanoparticles of Ag and Cu stacked on the biochar surface were spherical in shape with a particle size ranging from 25 to 45 nm. The potential for the removal of doxycycline (DOX) was explored, and it reached nearly 100% under optimum conditions, with the removal efficiency remaining at 81%, even after six consecutive regeneration cycles [237,238].

In another piece of work, a nanocomposite of pomelo peel loaded with Co and Fe was successfully prepared using an impregnation/co-precipitation method, used to activate peroxymonosulfate (PMS) for tetracycline removal. The activation mechanism of the PMS comprised free radical and non-free radical pathways put forward by EPR and quenching experiments, creating a potentially economically viable and highly efficient catalyst for PMS activation [239].

Jung et al. utilized a co-precipitation method followed by pyrolysis to synthesize a magnesium ferrite (MgFe_2O_4)/biochar composite and employed it to remove phosphate from water. The characterization studies completed revealed that the cubic spinel-shaped nanoparticles were successfully incorporated into the matrix of the biochar, providing magnetic separability with superparamagnetic behavior and authorizing a higher phosphate adsorption performance than that of primary biochar and only MgFe_2O_4 nanoparticles. A different piece of work by Wang et al. synthesized magnetic biochar by co-pyrolyzing halloysite and coconut shell at various temperatures. Halloysite/biochar and Fe_3O_4 were combined to create magnetic adsorbents, which were then assessed and compared for their ability to remove Pb (II) from water. The prepared sample exhibited an adsorption capacity of 833.33 ± 16.71 mg/g [240]. A magnetic biochar was synthesized by employing a microwave technology. The produced composite material had a specific surface area of $834 \text{ m}^2/\text{g}$, as reported by Yap et al., which exhibited an excellent ferromagnetic property for regeneration and poses high potential for Pb and Cd removal from wastewater at pH values of 4.5 and 4.8, respectively [241]. Using iron chloride in a simplified aqueous-phase method, along with pyrolysis at various peak temperatures ($450\text{--}650^\circ\text{C}$), Han et al. generated a magnetic biochar from peanut hull biomass [241,242]. The studies revealed that in contrast to ordinary biochar made from the same feedstock, the magnetic biochar demonstrated an exceptional capacity for the adsorption of Cr (VI) in aqueous solutions.

In summary, reducing biochar particles to micro-/nanoscale enhances adsorption capacities and multifunctionality due to large surface area-to-volume ratio, offering promising advancements in pollutant removal from water and soil systems. Furthermore, incorporating metal oxide nanoparticles such as ZnO or MgO into biochar improves the adsorption capacity and photocatalytic properties. Hybrid nanomaterials, such as Ag-Cu or Co-Fe, have also been utilized as active sites on biochar surfaces to create catalysts, demonstrating that biochar serves as a reliable and cost-effective support material for catalyst synthesis. Additionally, co-precipitating binary oxides like MgFe_2O_4 onto biochar results in nanocomposites with excellent ferromagnetic properties, which are particularly effective for heavy metal removal from aqueous systems. Finally, the modification of biochar at the nanoscale, along with the incorporation of metal oxides and hybrid nanomaterials, significantly enhances its adsorption, catalytic, and magnetic properties. These developments position biochar as a versatile and cost-effective material for environmental remediation.

6.3. Microbial Cell-Immobilized Biochar

The use of immobilized microbial biofilms for wastewater treatment and the bioremediation of organic and inorganic pollutants has been commonplace for a significant period of time. Hale et al. [243] proved the ability of biochar to serve as a microbial inoculum carrier. Living cells excrete polymeric materials that can attach and adhere to a biochar surface, developing an extracellular matrix called a microbial biofilm. The xenobiotic substrates undergo degradation by the genetic or metabolite exchanges facilitated by the biofilm-embedded cells [244]. Biofilms on a solid surface can resist mechanical stress to conserve microbial biomass [245].

Recent research has shown the enormous potential of using biochar and microorganisms for removing heavy metal ions and pesticides. Biochar can be used as an adsorbent for heavy metal ions and pesticides and as an immobilization support for microorganisms [246]. Microorganisms have higher biological activity on their surface areas, allowing them to adapt and survive in polluted areas through various strategies, such as surface adsorption, reduction, and enzymatic degradation [247]. Microorganisms can also remove heavy metal ions through biosorption and bioaccumulation, as well as through extracellular polymeric substance secretion, metallothionein synthesis, and biosurfactant production [248], as illustrated in Figure 5.

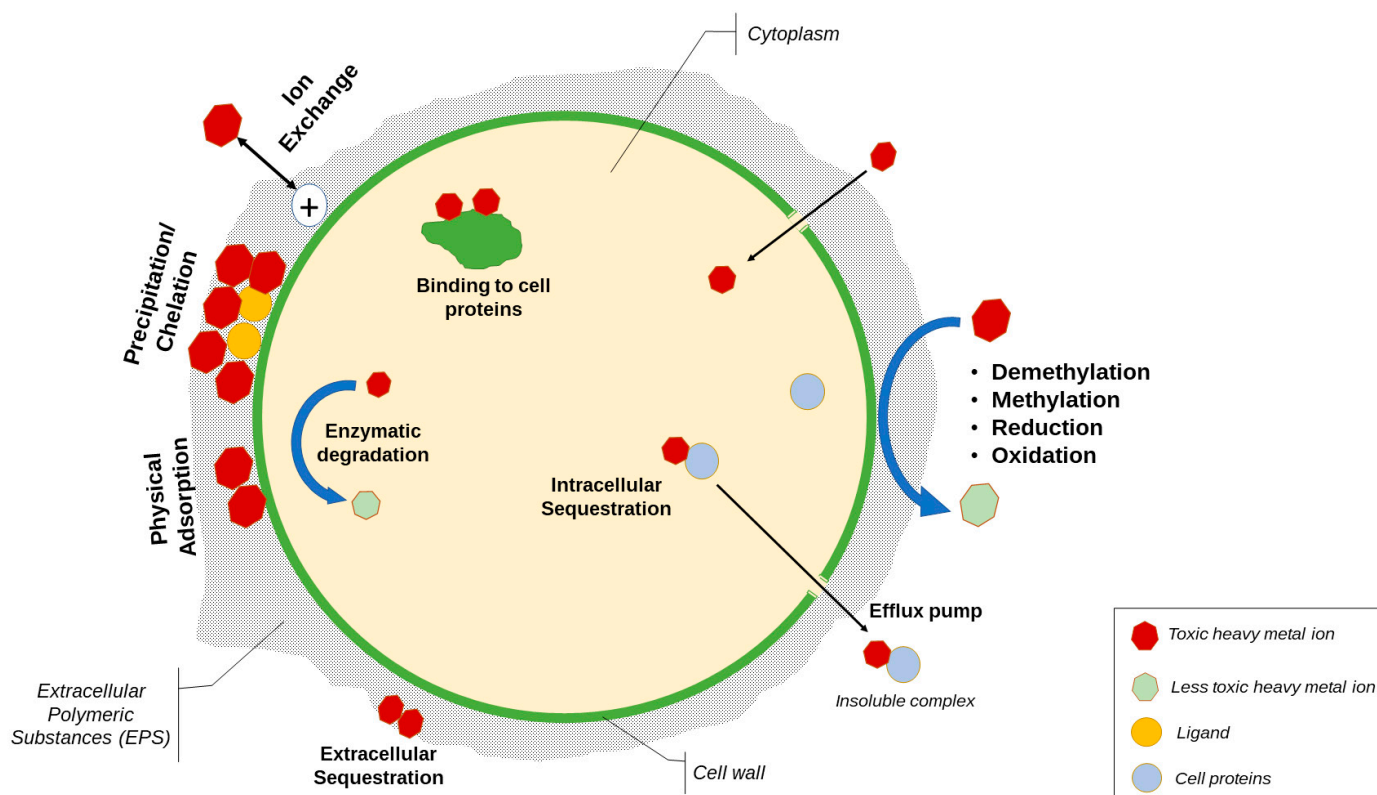


Figure 5. Mechanisms of heavy metal microbial bioremediation in a microbial cell (reproduced from [248,249]).

Biochar's porous structure promotes microbial growth and the adsorption of pollutants, reducing their concentration in soil/aqueous media [250]. In addition, immobilizing pollutant-degrading bacteria on biochar can enhance their survival and catalytic activity, leading to improved bioremediation of multiple contaminants [251]. Table 6 lists the microbial cell-immobilized biochars applied for different metal ion remediation situations. Among microbial communities, bacteria are the dominant culture used in the bioremediation of heavy metal ions.

The bioremediation of soil and water contaminated with lead has been a major focus due to the toxicity of the heavy metal. Teng et al. found that combining phosphate-solubilizing bacteria (PSB) and biochar led to the enhanced immobilization of Pb^{2+} through the formation of a stable crystal texture on its surface via electrostatic attraction and ion-exchange mechanisms [252]. Wang et al. conducted a study on the adsorption process of Pb^{2+} and Hg^{2+} on *Bacillus subtilis* loaded on biochar [253]. They found that cation- π interactions and precipitation contributed to this process. The study also revealed that the biochars were more efficient at adsorbing Pb^{2+} as compared to Hg^{2+} under similar conditions. The adsorption sites of Hg^{2+} and Pb^{2+} were found to partially overlap on the biochar surface but were different on co-sorbents. Chen et al. also employed PSB (*Enterobacter* sp.) to improve the biochar immobilization of Pb^{2+} in the solution [254], but their work showed a lower removal efficiency compared to that of Teng et al. [252].

The removal of Cd^{2+} was also examined using biochar-immobilized microalgae and bacteria. According to Shen et al., Cd^{2+} is removed through a combination of electrostatic attractions, surface complexation, and ion exchange [255]. Another heavy metal, hexavalent chromium ion, was completely removed from water by utilizing a *Proteus mirabilis* YC801 bacterial-algal biochar composite, as reported by Huang et al. [256]. Overall, the use of co-sorbents or microbe-biochar composites are more effective at removing heavy metal mixtures than biochar alone.

Table 6. Microbial cell-immobilized biochar for heavy metal remediation.

Metal	Microorganism		Biochar Source	Removal Efficiency	Reference
Pb	Bacteria	<i>Leclercia adecarboxylata</i>	Rice hull	93%	[252]
		<i>Bacillus subtilis</i>	Pig manure	112.3 mg/g	[253]
			Corn straw	83.0 mg/g	
		<i>Enterobacter</i> sp.	Rice husk	24.11%	[254]
			Sludge	60.85%	
		<i>Pseudomonas chlororaphis</i>	Cow dung	<1 mg/kg	[257]
Cd	Bacteria	<i>Bacillus</i> sp. TZ5	Coconut shell	48.49%	[258]
		<i>Delftia</i> sp. B9	Cornstalk	60.6–81.8%	[259]
	Algae	<i>Chlorella</i> sp.	Water hyacinth	92.5%	[255]
Cr *	Bacteria	<i>Proteus mirabilis</i> YC801	Bloom-forming cyanobacterium (D. flos-aquae)	100%	[256]
Cu	Bacteria	<i>Pseudomonas</i> sp. NT-2	Maize straw	Various	[260]
Mn	Bacteria	<i>Streptomyces violarus</i> strain SBP1	Raw and hydrogen peroxide-modified wood vinegar biochar	78%	[261]
Hg	Bacteria	<i>Bacillus subtilis</i>	Pig manure	69 mg/g	[253]
			Corn straw	53.7 mg/g	
Ni	Bacteria	<i>Pseudomonas stutzeri</i>	Sawdust	83%	[262]
U	Bacteria	<i>Bacillus subtilis</i> , <i>Bacillus cereus</i> , and <i>Citrobacter</i> sp.	Cornstalk Herb residue, cattle manure distillers’ grains, sugarcane bagasse	69%	[263]

* Hexavalent chromium ion (Cr⁶⁺).

6.4. Layered Structures

Layered double hydroxides (LDHs) are a type of bidimensional nanostructured material composed of positively charged layers of load-balanced metal hydroxides [264]. Through their lamellar structure, high porosity, large surface area, and high ion-exchange capacity, they are attractive adsorbent materials. In recent years, LDHs have been proposed in the literature as viable candidates for the removal of a range of pollutants from contaminated waters, including both organic and inorganic compounds. However, colloidal or nanometric adsorbents, such as LDHs, are more effective when supported or dispersed on porous substrates with a large surface area and low cost. Among these supporting materials, biochar stands out because it combines appropriate textural properties with broad environmental potential in terms of sustainability, low-cost production, and non-toxicity [265,266]. The synergistic action of LDHs with biochars has resulted in considerable improvements in the physicochemical properties of the resulting biochar/LDH composites, such as the specific surface area, surface functional groups, structural heterogeneity, stability and adsorption characteristics.

Over recent years, there has been considerable progress in the development of practical water remediation techniques, such as membrane separations, biological approaches, and adsorption. However, traditional water treatment materials, such as activated carbon, alumina, polymer resins, and silica gel zeolite have drawbacks, such as their high cost, low selectivity, complex regeneration, and low reusability performance. Biochar/LDH composites have emerged as fascinating materials because biochar can act as a low-cost, sustainable support matrix for the LDH and has been proven to efficiently remove harmful contaminants such as heavy metal ions, pesticides and volatile organic compounds [267,268]. Biochar/LDH's strong reusability performance may greatly cut the cost of the water treatment system process by employing cheaper alternatives. The porous biochar acts as a suitable support matrix, providing a large reactive area for effective metal hydroxide decorating and preventing LDH aggregation [269]. The surface functionalization, elemental composition, crystallographic structure, shape, and textural qualities of biochar/LDH composites are all significantly affected by the synthesis procedure [270]. Due to their tight structure, they are sensitive to structural collapse, which can limit their application as a form of water treatment. As previously mentioned, biochars can act as a suitable support matrix for LDHs, supporting the adsorption efficiency and overcoming the LDH deficiencies alone [271]. Due to the inclusion of the layered structure, the surface area of biochar affects the elimination of harmful contaminants, such as heavy metals, dyes, anions and pharmaceuticals [272]. The most utilized ways for producing biochar/LDH composites are the hydrothermal, co-precipitation, and co-pyrolysis methods. [267,268].

In one piece of work, Mg-Fe and Mg-Al (1:3)-layered double hydroxide (LDH)-coated bamboo biochar hybrids were synthesized using the liquid-phase co-precipitation approach for the removal of phosphate from aqueous solutions. The biochar composite with 40% Mg-Al LDH was able to achieve phosphate adsorption at >95% [273]. The biochar/LDH composite produced by Zhang and co-workers through the co-pyrolysis of biochar (Chinese cabbage and rape seeds) and MgAl-LDHs found that the Chinese rape biochar/MgAl exhibited better textural qualities than the Chinese cabbage biochar/MgAl and demonstrated quick phosphate ion elimination [274]. According to Huang et al., their MgAl/bamboo biochar has a lower adsorption capacity for Cr (VI) ions (38 mg/g) than MgAl/pinewood biochar (330.8 mg/g). The biochar feedstock and synthesis process clearly have a significant impact on the apparent difference in the Cr (VI) sorption capacity [275]. Furthermore, the type and nature of the divalent and trivalent cations in the LDH influence the physico-chemical properties of the biochar/LDH composite. MgAl/bamboo biochar, for example, has a greater affinity for phosphate ions than MgFe/bamboo biochar [273]. This is owing to MgAl's higher hydrophilicity compared to MgFe-LDH, which inhibits phosphate ion removal due to a lack of exposure to the biochar/MgFe sorption site. Another study found that a biochar/MgAl composite had a superior phosphate ion uptake capability while having a lower surface area than other LDHs (biochar/NiFe and biochar/ZnAl) [276].

Before the commercialization of biochar/LDH composites can take place, the potential environmental effects must be properly investigated. There is little evidence on the possible harmful effects of LDH/biochar composites, and more research in this area is needed to determine the viability of these adsorbents in real-world water treatment, such as metal leaching through sustained usage. On an industrial scale, the possibility of biochar/LDH composites as a cost-effective, efficient adsorbent must be investigated. A problem with this sustainable technology is ensuring cost-effectiveness, as, although they may be affordable at the laboratory scale, costs increase for mass-producing LDHs, biochar, and their composites. The existing synthesis approaches are primarily designed to produce a small quantity of biochar/LDH composites for laboratory use [272].

7. Conclusions

Biochars, lignocellulosic biomass waste-borne materials, are an economical, highly customizable (surface area, pore structure, surface functionalities and ability to generate composite materials) and environmentally attractive solution for heavy metal remediation from wastewater, especially those produced through industrial activities such as energy production and manufacturing. By being able to tune the uptake capabilities and capacities of biochars with alternative components, such as layered double hydroxides, membranes, or microbial cells, the mechanisms for pollutant removal can be promoted for metal species and metal ions in solution, including not only common pollutants such as Cu, Cr (multiple oxidation states), Fe, Cd, Mn, Hg, Ni, Co, and Pb but also U and phosphates. The mechanisms investigated include ion exchange, electrostatic physisorption through surface functionalities (subject to pH), hydrogen bonding, precipitation, physical adsorption, complexation and pore filling. Each removal strategy can utilize different kinetic pathways, subject to the conditions used or the state of the adsorption sites.

The regeneration potential of biochar further improves its economic viability and long-term environmental sustainability after post-processing to remove the stored pollutants using thermal, microwave, physicochemical and chemical methods, as well as biochars have been shown to maintain high extraction capabilities after several cycles. However, the use of supercritical fluids for regeneration is not seen as economically viable now, due to it being in the infancy stage and the relatively high capex requirements.

The operation and maintenance of active/closed mines, as an example, lead to sediment pollution through the contamination of soil, mine tailings, wastewater and sometimes groundwater. The soil pH surrounding the site affects how heavy metals travel in the environment (infiltration), which can lead to variation in heavy metal concentrations. Biochars are able to operate across all pH conditions, and it has been found that preferential metal uptake can be found at specific pH values for different metal pollutants, allowing for selective extraction. The release of wastewater from manufacturing sites is another route for heavy metals to enter local water systems. The wider literature reports samples being taken from manufacturing parks, and the concentrations of some heavy metals have been found to exceed the international quality guidelines, even with the current water treatment in place. Thus, further refinement is needed to improve the process. Underground geothermal fluids naturally contain dissolved solids, and the chemical composition is dependent on the geothermal fields. However, the anthropogenic utilization of these fluids for energy production, especially in processes like fluid flashing in geothermal plants, may result in increased concentrations when the water is recycled or reused for aboveground applications. Another energy industry that can cause heavy metal pollution is fracking. This occurs by the contamination of soil and groundwater due to the fracking chemicals used or the flowback water. Similar to what was identified for mining and manufacturing, the concentrations of heavy metals varied from report to report. To successfully apply biochar to industrial applications for wastewater treatment, the impact of the flow rate on the adsorption for continuous processing needs to be considered. It has been discussed that there is an inverse relationship between the flow rate and adsorption capacity, leading to a decrease in the adsorption as the flow rate increases. However, the functionalities and expansive pore networks available from the various biochars and biochar composite materials do provide multiple adsorption mechanisms. These have not been fully exploited yet for industrial gains; however, they have been clearly showcased under batch conditions to great effect.

Funding: P: SKM and MJT acknowledge the Commonwealth Scholarship Commission for P's Split-Site Scholarship 2022 (INCN-2022-395). This work was supported by the Engineering and Physical Sciences Research Council and the Natural Environment Research Council EP/S023763/1, the EPSRC Centre for Doctoral Training in Offshore Wind Energy.

Conflicts of Interest: The authors declare no conflict of interest.

References

- Rivera, A.; Movalia, S.; Rutkowski, E.; Rangel, Y.; Pitt, H.; Larsen, K. Global Greenhouse Gas Emissions: 1990–2021 and Preliminary 2022 Estimates. Available online: <https://rhg.com/research/global-greenhouse-gas-emissions-2022/> (accessed on 18 September 2024).
- Friedlingstein, P.; Jones, M.W.; O’Sullivan, M.; Andrew, R.M.; Bakker, D.C.E.; Hauck, J.; Le Quéré, C.; Peters, G.P.; Peters, W.; Pongratz, J.; et al. Global Carbon Budget 2021. *Earth Syst. Sci. Data* **2022**, *14*, 1917–2005. [\[CrossRef\]](#)
- IRENA. *Decarbonising Hard-to-Abate Sectors with Renewables: Perspectives for the G7*; International Renewable Energy Agency (IRENA): Abu Dhabi, United Arab Emirates, 2024.
- Chin, J.F.; Heng, Z.W.; Teoh, H.C.; Chong, W.C.; Pang, Y.L. Recent development of magnetic biochar crosslinked chitosan on heavy metal removal from wastewater—Modification, application and mechanism. *Chemosphere* **2022**, *291*, 133035. [\[CrossRef\]](#)
- Kannappan, S.; Ramisetty, B.C.M. Engineered Whole-Cell-Based Biosensors: Sensing Environmental Heavy Metal Pollutants in Water—A Review. *Appl. Biochem. Biotechnol.* **2022**, *194*, 1814–1840. [\[CrossRef\]](#)
- IEA. *Net Zero by 2050*; International Energy Agency (IEA): Paris, France, 2021.
- Moreno-Sader, K.; García-Padilla, A.; Realpe, A.; Acevedo-Morantes, M.; Soares, J.B.P. Removal of Heavy Metal Water Pollutants (Co²⁺ and Ni²⁺) Using Polyacrylamide/Sodium Montmorillonite (PAM/Na-MMT) Nanocomposites. *ACS Omega* **2019**, *4*, 10834–10844. [\[CrossRef\]](#)
- Jin, X.; Yu, C.; Li, Y.; Qi, Y.; Yang, L.; Zhao, G.; Hu, H. Preparation of novel nano-adsorbent based on organic–inorganic hybrid and their adsorption for heavy metals and organic pollutants presented in water environment. *J. Hazard. Mater.* **2011**, *186*, 1672–1680. [\[CrossRef\]](#)
- Ho, S.-H.; Zhu, S.; Chang, J.-S. Recent advances in nanoscale-metal assisted biochar derived from waste biomass used for heavy metals removal. *Bioresour. Technol.* **2017**, *246*, 123–134. [\[CrossRef\]](#)
- Alengebawy, A.; Abdelkhalek, S.T.; Qureshi, S.R.; Wang, M.Q. Heavy Metals and Pesticides Toxicity in Agricultural Soil and Plants: Ecological Risks and Human Health Implications. *Toxics* **2021**, *9*, 42. [\[CrossRef\]](#) [\[PubMed\]](#)
- Vashisht, D.; Taylor, M.J.; Mehta, S.K. Evaluating the pre-treatment protocol required to produce an effective carbonized waste adsorbent for organic pollution control. *Front. Environ. Sci.* **2023**, *11*, 1224388. [\[CrossRef\]](#)
- Islam, M.S.; Kwak, J.-H.; Nzediegwu, C.; Wang, S.; Palansuriya, K.; Kwon, E.E.; Naeth, M.A.; El-Din, M.G.; Ok, Y.S.; Chang, S.X. Biochar heavy metal removal in aqueous solution depends on feedstock type and pyrolysis purging gas. *Environ. Pollut.* **2021**, *281*, 117094. [\[CrossRef\]](#)
- Priyanka Vashisht, D.; Ibhaddon, A.O.; Mehta, S.K.; Taylor, M.J. Enhanced Wastewater Remediation Using Mesoporous Activated Wheat Straw Biochars: A Dye Removal Perspective. *ACS Sustain. Resour. Manag.* **2024**, *1*, 355–367. [\[CrossRef\]](#)
- Yaashikaa, P.R.; Kumar, P.S.; Varjani, S.; Saravanan, A. A critical review on the biochar production techniques, characterization, stability and applications for circular bioeconomy. *Biotechnol. Rep.* **2020**, *28*, e00570. [\[CrossRef\]](#)
- Nor Adilla, R.; Suzana, Y. A Mini Review of Biochar Synthesis, Characterization, and Related Standardization and Legislation. In *Applications of Biochar for Environmental Safety*; Ahmed, A.A., Mohammed, H.H.A., Eds.; IntechOpen: Rijeka, Croatia, 2020. [\[CrossRef\]](#)
- Belmont, E.; Sanchez, D.L.; Smith, P.; Torn, M. The Building Blocks of CDR Systems: Biochar. In *CDR Primer*; Wilcox, J., Kolosz, B., Freeman, J., Eds.; IntechOpen: Rijeka, Croatia, 2021.
- Lehmann, J.; Kuzyakov, Y.; Pan, G.; Ok, Y.S. Biochars and the plant-soil interface. *Plant Soil* **2015**, *395*, 1–5. [\[CrossRef\]](#)
- Campbell, J.L.; Sessions, J.; Smith, D.; Trippe, K. Potential carbon storage in biochar made from logging residue: Basic principles and Southern Oregon case studies. *PLoS ONE* **2018**, *13*, e0203475. [\[CrossRef\]](#)
- Spokas, K.A. Review of the stability of biochar in soils: Predictability of O:C molar ratios. *Carbon Manag.* **2010**, *1*, 289–303. [\[CrossRef\]](#)
- Santos, V.B.; Araújo, A.S.F.; Leite, L.F.C.; Nunes, L.A.P.L.; Melo, W.J. Soil microbial biomass and organic matter fractions during transition from conventional to organic farming systems. *Geoderma* **2012**, *170*, 227–231. [\[CrossRef\]](#)
- Hammes, F.; Berney, M.; Wang, Y.; Vital, M.; Köster, O.; Egli, T. Flow-cytometric total bacterial cell counts as a descriptive microbiological parameter for drinking water treatment processes. *Water Res.* **2008**, *42*, 269–277. [\[CrossRef\]](#)
- National Academies of Sciences Engineering and Medicine. *Negative Emissions Technologies and Reliable Sequestration: A Research Agenda*; The National Academies Press: Washington, DC, USA, 2019. [\[CrossRef\]](#)
- Jeffery, S.; Abalos, D.; Prodana, M.; Bastos, A.; Van Groenigen, J.W.; Hungate, B.; Verheijen, F. Biochar boosts tropical but not temperate crop yields. *Environ. Res. Lett.* **2017**, *12*, 053001. [\[CrossRef\]](#)
- Wang, J.; Xiong, Z.; Kuzyakov, Y. Biochar stability in soil: Meta-analysis of decomposition and priming effects. *Gcb Bioenergy* **2015**, *8*, 512–523. [\[CrossRef\]](#)
- Ippolito, J.A.; Cui, L.; Kammann, C.; Wrage-Mönnig, N.; Estavillo, J.M.; Fuertes-Mendizabal, T.; Cayuela, M.L.; Sigua, G.; Novak, J.; Spokas, K.; et al. Feedstock choice, pyrolysis temperature and type influence biochar characteristics: A comprehensive meta-data analysis review. *Biochar* **2020**, *2*, 421–438. [\[CrossRef\]](#)
- Lee, M.; Lin, Y.-L.; Chiueh, P.-T.; Den, W. Environmental and energy assessment of biomass residues to biochar as fuel: A brief review with recommendations for future bioenergy systems. *J. Clean. Prod.* **2020**, *251*, 119714. [\[CrossRef\]](#)
- United Nations Environment Programme. *Food Waste Index Report 2021*; United Nations Environment Programme (UNEP): Nairobi, Kenya, 2021.

28. Zilberman, D.; Laird, D.; Rainey, C.; Song, J.; Kahn, G. Biochar supply-chain and challenges to commercialization. *GCB-Bioenergy* **2022**, *15*, 7–23. [\[CrossRef\]](#)
29. Russell, S. *Estimating and Reporting the Comparative Impacts of Products*; World Resources Institute: Washington, DC, USA, 2019.
30. Griscom, B.; Adams, J.; Ellis, P.; Houghton, R.; Lomax, G.; Miteva, D.; Schlesinger, W.; Shoch, D.; Siikamäki, J.; Smith, P.; et al. Natural climate solutions. *Proc. Natl. Acad. Sci. USA* **2017**, *114*, 11645–11650. [\[CrossRef\]](#)
31. Paustian, K.; Lehmann, J.; Ogle, S.; Reay, D.; Robertson, G.P.; Smith, P. Climate-smart soils. *Nature* **2016**, *532*, 49–57. [\[CrossRef\]](#)
32. Woolf, D.; Amonette, J.E.; Street-Perrott, F.A.; Lehmann, J.; Joseph, S. Sustainable biochar to mitigate global climate change. *Nat. Commun.* **2010**, *1*, 56. [\[CrossRef\]](#)
33. Laird, D.A. The charcoal vision: A win-win-win scenario for simultaneously producing bioenergy, permanently sequestering carbon, while improving soil and water quality. *Agron. J.* **2008**, *100*, 178–181. [\[CrossRef\]](#)
34. Cayuela, M.L.; Van Zwieten, L.; Singh, B.P.; Jeffery, S.; Roig, A.; Sánchez-Monedero, M. Biochar's role in mitigating soil nitrous oxide emissions: A review and meta-analysis. *Agric. Ecosyst. Environ.* **2014**, *191*, 5–16. [\[CrossRef\]](#)
35. Matušík, J.; Hnátková, T.; Kočí, V. Life cycle assessment of biochar-to-soil systems: A review. *J. Clean. Prod.* **2020**, *259*, 120998. [\[CrossRef\]](#)
36. Wilcox, J.; Kolosz, B.; Freeman, J. *Carbon Dioxide Removal Primer*, 1st ed.; IntechOpen: Rijeka, Croatia, 2021.
37. Lehmann, J.; Gaunt, J.; Rondon, M. Bio-char Sequestration in Terrestrial Ecosystems—A Review. *Mitig. Adapt. Strateg. Glob. Chang.* **2006**, *11*, 403–427. [\[CrossRef\]](#)
38. Lehmann, J. Bio-energy in the black. *Front. Ecol. Environ.* **2007**, *5*, 381–387. [\[CrossRef\]](#)
39. Kumar, A.; Bhattacharya, T. Biochar: A sustainable solution. *Environ. Dev. Sustain.* **2021**, *23*, 6642–6680. [\[CrossRef\]](#)
40. Weng, Z.; Van Zwieten, L.; Singh, B.P.; Tavakkoli, E.; Joseph, S.; Macdonald, L.M.; Rose, T.J.; Rose, M.T.; Kimber, S.W.L.; Morris, S.; et al. Biochar built soil carbon over a decade by stabilizing rhizodeposits. *Nat. Clim. Change* **2017**, *7*, 371–376. [\[CrossRef\]](#)
41. Lehmann, J.; Rillig, M.C.; Thies, J.; Masiello, C.A.; Hockaday, W.C.; Crowley, D. Biochar effects on soil biota—a review. *Soil Biol. Biochem.* **2011**, *43*, 1812–1836. [\[CrossRef\]](#)
42. Masiello, C.; Dugan, B.; Brewer, C.; Spokas, K.; Novak, J.; Liu, Z.; Sorrenti, G. Biochar effects on soil hydrology. In *Biochar for Environmental Management*; Earthscan from Routledge: London, UK, 2015; Volume 2, pp. 541–560.
43. Liang, B.; Lehmann, J.; Solomon, D.; Kinyangi, J.; Grossman, J.; O'Neill, B.; Skjemstad, J.O.; Thies, J.; Luizão, F.J.; Petersen, J.; et al. Black carbon increases cation exchange capacity in soils. *Soil Sci. Soc. Am. J.* **2006**, *70*, 1719–1730. [\[CrossRef\]](#)
44. Laird, D.; Fleming, P.; Wang, B.; Horton, R.; Karlen, D. Biochar impact on nutrient leaching from a Midwestern agricultural soil. *Geoderma* **2010**, *158*, 436–442. [\[CrossRef\]](#)
45. Elad, Y.; David, D.R.; Harel, Y.M.; Borenshtein, M.; Kalifa, H.B.; Silber, A.; Graber, E.R. Induction of systemic resistance in plants by biochar, a soil-applied carbon sequestering agent. *Phytopathology* **2010**, *100*, 913–921. [\[CrossRef\]](#)
46. Beesley, L.; Moreno-Jiménez, E.; Gomez-Eyles, J.L.; Harris, E.; Robinson, B.; Sizmur, T. A review of biochars' potential role in the remediation, revegetation and restoration of contaminated soils. *Environ. Pollut.* **2011**, *159*, 3269–3282. [\[CrossRef\]](#)
47. Hale, S.; Hanley, K.; Lehmann, J.; Zimmerman, A.; Cornelissen, G. Effects of chemical, biological, and physical aging as well as soil addition on the sorption of pyrene to activated carbon and biochar. *Environ. Sci. Technol.* **2011**, *45*, 10445–10453. [\[CrossRef\]](#)
48. Spokas, K.A.; Novak, J.M.; Venterea, R.T. Biochar's role as an alternative N-fertilizer: Ammonia capture. *Plant Soil* **2012**, *350*, 35–42. [\[CrossRef\]](#)
49. Crane-Droesch, A.; Abiven, S.; Jeffery, S.; Torn, M. Heterogeneous global crop yield response to biochar: A meta-regression analysis. *Environ. Res. Lett.* **2013**, *8*, 044049. [\[CrossRef\]](#)
50. Whitman, T.; Nicholson, C.F.; Torres, D.; Lehmann, J. Climate change impact of biochar cook stoves in Western Kenyan farm households: System dynamics model analysis. *Environ. Sci. Technol.* **2011**, *45*, 3687–3694. [\[CrossRef\]](#)
51. Vassilev, S.V.; Baxter, D.; Andersen, L.K.; Vassileva, C.G. An overview of the composition and application of biomass ash. part 1. phase—mineral and chemical composition and classification. *Fuel* **2013**, *105*, 40–76. [\[CrossRef\]](#)
52. Vassilev, S.V.; Baxter, D.; Andersen, L.K.; Vassileva, C.G.; Morgan, T.J. An overview of the organic and inorganic phase composition of biomass. *Fuel* **2012**, *94*, 1–33. [\[CrossRef\]](#)
53. Gezae, A.; Chandraratne, M. Biochar production from biomass waste-derived material. *Biochar Prod. Biomass Waste-Deriv. Mater.* **2018**, *4*, 370–378. [\[CrossRef\]](#)
54. Jafri, N.; Wong, W.Y.; Doshi, V.; Yoon, L.W.; Cheah, K.H. A review on production and characterization of biochars for application in direct carbon fuel cells. *Process Saf. Environ. Prot.* **2018**, *118*, 152–166. [\[CrossRef\]](#)
55. Hendriks, A.T.W.M.; Zeeman, G. Pretreatments to enhance the digestibility of lignocellulosic biomass. *Bioresour. Technol.* **2009**, *100*, 10–18. [\[CrossRef\]](#)
56. Taylor, M.; Alabdrabameer, H.; Skoulou, V. Choosing Physical, Physicochemical and Chemical Methods of Pre-Treating Lignocellulosic Wastes to Repurpose into Solid Fuels. *Sustainability* **2019**, *11*, 3604. [\[CrossRef\]](#)
57. Brethauer, S.; Shahab, R.L.; Studer, M.H. Impacts of biofilms on the conversion of cellulose. *Appl. Microbiol. Biotechnol.* **2020**, *104*, 5201–5212. [\[CrossRef\]](#)
58. Isikgor, F.H.; Becer, C.R. Lignocellulosic biomass: A sustainable platform for the production of bio-based chemicals and polymers. *Polym. Chem.* **2015**, *6*, 4497–4559. [\[CrossRef\]](#)
59. Wang, J.; Wang, S. Preparation, modification and environmental application of biochar: A Review. *J. Clean. Prod.* **2019**, *227*, 1002–1022. [\[CrossRef\]](#)

60. Castro, R.I.; Morales-Quintana, L. Study of the cell wall components produced during different ripening stages through thermogravimetric analysis. *Cellulose* **2019**, *26*, 3009–3020. [\[CrossRef\]](#)
61. Haiping, Y.; Yan, R.; Chen, H.; Lee, D.; Zheng, C. Characteristics of hemicellulose, cellulose and lignin pyrolysis. *Fuel* **2007**, *86*, 1781–1788. [\[CrossRef\]](#)
62. Lee, J.; Sohn, D.; Lee, K.; Park, K.Y. Solid fuel production through hydrothermal carbonization of sewage sludge and microalgae *Chlorella* sp. from wastewater treatment plant. *Chemosphere* **2019**, *230*, 157–163. [\[CrossRef\]](#)
63. De Bhowmick, G.; Sarmah, A.K.; Sen, R. Zero-waste algal biorefinery for bioenergy and biochar: A green leap towards achieving energy and environmental sustainability. *Sci. Total Environ.* **2019**, *650*, 2467–2482. [\[CrossRef\]](#)
64. Cha, J.S.; Park, S.H.; Jung, S.-C.; Ryu, C.; Jeon, J.-K.; Shin, M.-C.; Park, Y.-K. Production and utilization of biochar: A Review. *J. Ind. Eng. Chem.* **2016**, *40*, 1–15. [\[CrossRef\]](#)
65. Cheah, S.; Malone, S.C.; Feik, C.J. Speciation of sulfur in biochar produced from pyrolysis and gasification of oak and corn stover. *Environ. Sci. Technol.* **2014**, *48*, 8474–8480. [\[CrossRef\]](#)
66. Neogi, S.; Sharma, V.; Khan, N.; Chaurasia, D.; Ahmad, A.; Chauhan, S.; Singh, A.; You, S.; Pandey, A.; Bhargava, P.C. Sustainable biochar: A facile strategy for soil and environmental restoration, energy generation, mitigation of global climate change and circular bioeconomy. *Chemosphere* **2022**, *293*, 133474. [\[CrossRef\]](#)
67. Oyedun, A.O.; Gebreegziabher, T.; Hui, C.W. Mechanism and modelling of bamboo pyrolysis. *Fuel Process. Technol.* **2013**, *106*, 595–604. [\[CrossRef\]](#)
68. Goyal, H.B.; Seal, D.; Saxena, R.C. Bio-fuels from thermochemical conversion of renewable resources: A review. *Renew. Sustain. Energy Rev.* **2008**, *12*, 504–517. [\[CrossRef\]](#)
69. Al-Rumaihi, A.; Shahbaz, M.; McKay, G.; Mackey, H.; Al-Ansari, T. A review of pyrolysis technologies and feedstock: A blending approach for plastic and biomass towards optimum biochar yield. *Renew. Sustain. Energy Rev.* **2022**, *167*, 112715. [\[CrossRef\]](#)
70. Laird, D.A.; Brown, R.C.; Amonette, J.E.; Lehmann, J. Review of the pyrolysis platform for coproducing bio-oil and biochar. *Biofuels Bioprod. Biorefin.* **2009**, *3*, 547–562. [\[CrossRef\]](#)
71. Niu, S.; Xia, Y.; Yang, C.; Liu, C. Impacts of the steel industry on sediment pollution by heavy metals in urban water system. *Environ. Pollut.* **2023**, *335*, 122364. [\[CrossRef\]](#)
72. Puga, A.P.; Melo, L.C.A.; de Abreu, C.A.; Coscione, A.R.; Paz-Ferreiro, J. Leaching and fractionation of heavy metals in mining soils amended with biochar. *Soil. Tillage Res.* **2016**, *164*, 25–33. [\[CrossRef\]](#)
73. Ghosh, D.; Maiti, S. Biochar assisted phytoremediation and biomass disposal in heavy metal contaminated mine soils: A review. *Int. J. Phytoremediat.* **2021**, *23*, 559–576. [\[CrossRef\]](#)
74. Mendez, M.O.; Maier, R.M. Phytostabilization of mine tailings in arid and semiarid environments—An emerging remediation technology. *Environ. Health Perspect.* **2008**, *116*, 278–283. [\[CrossRef\]](#)
75. Chen, G.C.; He, Z.L.; Stoffella, P.J.; Yang, X.E.; Yu, S.; Yang, J.Y.; Calvert, D.V. Leaching potential of heavy metals (Cd, Ni, Pb, Cu and Zn) from acidic sandy soil amended with dolomite phosphate rock (DPR) fertilizers. *J. Trace Elem. Med. Biol.* **2006**, *20*, 127–133. [\[CrossRef\]](#)
76. Jiang, C.; Zhao, Q.; Zheng, L.; Chen, X.; Li, C.; Ren, M. Distribution, source and health risk assessment based on the Monte Carlo method of heavy metals in shallow groundwater in an area affected by mining activities, China. *Ecotoxicol. Environ. Saf.* **2021**, *224*, 112679. [\[CrossRef\]](#)
77. Mahato, M.K.; Singh, G.; Singh, P.K.; Singh, A.K.; Tiwari, A.K. Assessment of Mine Water Quality Using Heavy Metal Pollution Index in a Coal Mining Area of Damodar River Basin, India. *Bull. Environ. Contam. Toxicol.* **2017**, *99*, 54–61. [\[CrossRef\]](#)
78. Kim, D.-M.; Yun, S.-T.; Cho, Y.; Hong, J.-H.; Batsaikhan, B.; Oh, J. Hydrochemical assessment of environmental status of surface and ground water in mine areas in South Korea: Emphasis on geochemical behaviors of metals and sulfate in ground water. *J. Geochem. Explor.* **2017**, *183*, 33–45. [\[CrossRef\]](#)
79. Khafouri, A.; Talbi, E.H.; Abdelouas, A. Assessment of Heavy Metal Contamination of the Environment in the Mining Site of Ouixane (North East Morocco). *Water Air Soil Pollut.* **2021**, *232*, 398. [\[CrossRef\]](#)
80. Gyamfi, E.; Appiah-Adjei, E.K.; Adjei, K.A. Potential heavy metal pollution of soil and water resources from artisanal mining in Kokoteasua, Ghana. *Groundw. Sustain. Dev.* **2019**, *8*, 450–456. [\[CrossRef\]](#)
81. Noli, F.; Tsamos, P. Seasonal variations of natural radionuclides, minor and trace elements in lake sediments and water in a lignite mining area of North-Western Greece. *Environ. Sci. Pollut. Res. Int.* **2018**, *25*, 12222–12233. [\[CrossRef\]](#)
82. Ippolito, J.A.; Berry, C.M.; Strawn, D.G.; Novak, J.M.; Levine, J.; Harley, A. Biochars reduce mine land soil bioavailable metals. *J. Environ. Qual.* **2017**, *46*, 411–419. [\[CrossRef\]](#)
83. Bandara, T.; Xu, J.; Potter, I.D.; Franks, A.; Chathurika, J.B.A.J.; Tang, C. Mechanisms for the removal of Cd (II) and Cu (II) from aqueous solution and mine water by biochars derived from agricultural wastes. *Chemosphere* **2020**, *254*, 126745. [\[CrossRef\]](#)
84. Álvarez, M.L.; Gascó, G.; Rodríguez-Pacheco, R.; Paz-Ferreiro, J.; Méndez, A. Recovery of metals from mine wastes: The effect of biochar-Fe composites in the immobilization of arsenic. *J. Sustain. Metall.* **2022**, *8*, 419–429. [\[CrossRef\]](#)
85. Barragán-Mantilla, S.P.; Gascó, G.; Méndez, A. Perspectives on the use of biochar in the valorization of mining wastes from sulfide minerals flotation: Recovery of metals and effects on toxicity. *Waste Manag.* **2023**, *171*, 116–123. [\[CrossRef\]](#)
86. Zhang, Q.; Song, Y.; Amor, K.; Huang, W.E.; Porcelli, D.; Thompson, I. Monitoring Cr toxicity and remediation processes—Combining a whole-cell bioreporter and Cr isotope techniques. *Water Res.* **2019**, *153*, 295–303. [\[CrossRef\]](#)

87. Emamverdian, A.; Ding, Y.; Barker, J.; Liu, G.; Li, Y.; Mokhberdoran, F. Sodium Nitroprusside Improves Bamboo Resistance under Mn and Cr Toxicity with Stimulation of Antioxidants Activity, Relative Water Content, and Metal Translocation and Accumulation. *Int. J. Mol. Sci.* **2023**, *24*, 1942. [\[CrossRef\]](#)
88. Beesley, L.; Marmiroli, M. The immobilisation and retention of soluble arsenic, cadmium and zinc by biochar. *Environ. Pollut.* **2011**, *159*, 474–480. [\[CrossRef\]](#)
89. Chen, J.; Deng, S.; Jia, W.; Li, X.; Chang, J. Removal of multiple heavy metals from mining-impacted water by biochar-filled constructed wetlands: Adsorption and biotic removal routes. *Bioresour. Technol.* **2021**, *331*, 125061. [\[CrossRef\]](#)
90. Levinson, M. *What Is Manufacturing? Why Does the Definition Matter?* National Institute of Standards and Technology (NIST): Gaithersburg, MD, USA, 2017; pp. 1–14.
91. Rohdin, P.; Thollander, P. Barriers to and driving forces for energy efficiency in the non-energy intensive manufacturing industry in Sweden. *Energy* **2006**, *31*, 1836–1844. [\[CrossRef\]](#)
92. Liu, R.; Tan, R.; Li, B.; Song, Y.; Zeng, P.; Li, Z. Overview of POPs and heavy metals in Liao River Basin. *Environ. Earth Sci.* **2015**, *73*, 5007–5017. [\[CrossRef\]](#)
93. Hsu, S.C.; Hsieh, H.L.; Chen, C.P.; Tseng, C.M.; Huang, S.C.; Huang, C.H.; Huang, Y.T.; Radashevsky, V.; Lin, S.H. Tungsten and other heavy metal contamination in aquatic environments receiving wastewater from semiconductor manufacturing. *J. Hazard. Mater.* **2011**, *189*, 193–202. [\[CrossRef\]](#)
94. Karthikeyan, S.; Arumugam, S.; Muthumanickam, J.; Kulandaisamy, P.; Subramanian, M.; Annadurai, R.; Senapathi, V.; Sekar, S. Causes of heavy metal contamination in groundwater of Tuticorin industrial block, Tamil Nadu, India. *Environ. Sci. Pollut. Res. Int.* **2021**, *28*, 18651–18666. [\[CrossRef\]](#) [\[PubMed\]](#)
95. Meme, F.K.; Nwadukwe, F.O. Impact Assessment of Cement Factory Waste Water on the Heavy Metal Contents of a Typical Low-Latitude Stream in North Central Nigeria. *Int. Inst. Sci. Technol. Educ. (IISTE)* **2016**, *8*, 42–48.
96. Noreen, U.; Ahmed, Z.; Khalid, A.; Di Serafino, A.; Habiba, U.; Ali, F.; Hussain, M. Water pollution and occupational health hazards caused by the marble industries in district Mardan, Pakistan. *Environ. Technol. Innov.* **2019**, *16*, 100470. [\[CrossRef\]](#)
97. Watson, A. *Geothermal Engineering*, 1st ed.; Springer: New York, NY, USA, 2016. [\[CrossRef\]](#)
98. Durowoju, O.; Odiyo, J.; Ekosse, G.-I. Hydrogeochemical setting of geothermal springs in Limpopo Province, South Africa. *Res. J. Chem. Environ.* **2015**, *19*, 82–93.
99. Odiyo, J.; Makungo, R. Fluoride concentrations in groundwater and impact on human health in Siloam Village, Limpopo Province, South Africa. *Water SA* **2011**, *38*, 731–736. [\[CrossRef\]](#)
100. Rapoliene, L.; Razbadauskas, A.; Jurgelenas, A. The reduction of distress using therapeutic geothermal water procedures in a randomized controlled clinical trial. *Adv. Prev. Med.* **2015**, *2015*, 749417. [\[CrossRef\]](#)
101. Nivetha, A.; Sakthivel, C.; Prapha, I. Heavy Metal Contamination in Groundwater and Impact on Plant and Human. In *Spatial Modeling and Assessment of Environmental Contaminants*; Springer: Berlin, Germany, 2021; pp. 233–246. [\[CrossRef\]](#)
102. Clark, C.E.; Harto, C.B.; Sullivan, J.L.; Wang, M.Q. *Water Use in the Development and Operation of Geothermal Power Plants*; Argonne National Laboratory: Argonne, IL, USA, 2010.
103. Finster, M.; Clark, C.; Schroeder, J.; Martino, L. Geothermal produced fluids: Characteristics, treatment technologies, and management options. *Renew. Sustain. Energy Rev.* **2015**, *50*, 952–966. [\[CrossRef\]](#)
104. Stoljarova, A.; Regenspurg, S.; Bäßler, R.; Mathiesen, T.; Nielsen, J.B. Effect of lead and copper containing brine on steel materials for geothermal applications—A corrosion study. *Geothermics* **2021**, *91*, 102024. [\[CrossRef\]](#)
105. Collin, S.; Baskar, A.; Geevarghese, D.M.; Ali, M.N.V.S.; Bahubali, P.; Choudhary, R.; Lvov, V.; Tovar, G.I.; Senatov, F.; Koppala, S.; et al. Bioaccumulation of lead (Pb) and its effects in plants: A review. *J. Hazard. Mater. Lett.* **2022**, *3*, 100064. [\[CrossRef\]](#)
106. Zulfiqar, U.; Farooq, M.; Hussain, S.; Maqsood, M.; Hussain, M.; Ishfaq, M.; Ahmad, M.; Anjum, M.Z. Lead toxicity in plants: Impacts and remediation. *J. Environ. Manag.* **2019**, *250*, 109557. [\[CrossRef\]](#) [\[PubMed\]](#)
107. Kunan, P.; Ravier, G.; Dalmais, E.; Ducouso, M.; Cezac, P. Thermodynamic and Kinetic Modelling of Scales Formation at the Soultz-sous-Forêts Geothermal Power Plant. *Geosciences* **2021**, *11*, 483. [\[CrossRef\]](#)
108. Brown, K. Antimony and Arsenic Sulfide Scaling in Geothermal Binary Plants. In Proceedings of the International Workshop on Mineral Scaling 2011, Manila, Philippines, 25–27 May 2011; pp. 103–106.
109. Kayode, O.T.; Aizebeokhai, A.P.; Odukoya, A.M. Arsenic in agricultural soils and implications for sustainable agriculture. *IOP Conf. Ser. Earth Environ. Sci.* **2021**, *655*, 012081. [\[CrossRef\]](#)
110. Ravenscroft, P.; Brammer, H.; Richards, K. *Arsenic Pollution: A Global Synthesis*; Springer: Berlin/Heidelberg, Germany, 2009; Volume 1.
111. Parisi, M.L.; Ferrara, N.; Torsello, L.; Basosi, R. Life cycle assessment of atmospheric emission profiles of the Italian geothermal power plants. *J. Clean. Prod.* **2019**, *234*, 881–894. [\[CrossRef\]](#)
112. Zhang, Y.; Song, Z.; Huang, S.; Zhang, P.; Peng, Y.; Wu, P.; Gu, J.; Dutkiewicz, S.; Zhang, H.; Wu, S.; et al. Global health effects of future atmospheric mercury emissions. *Nat. Commun.* **2021**, *12*, 3035. [\[CrossRef\]](#) [\[PubMed\]](#)
113. Ellis, A.J. Geothermal fluid chemistry and human health. *Geothermics* **1977**, *6*, 175–182. [\[CrossRef\]](#)
114. Driscoll, C.T.; Mason, R.P.; Chan, H.M.; Jacob, D.J.; Pirrone, N. Mercury as a Global Pollutant: Sources, Pathways, and Effects. *Environ. Sci. Technol.* **2013**, *47*, 4967–4983. [\[CrossRef\]](#) [\[PubMed\]](#)
115. Smith, D.G. *Heavy Metals in the New Zealand Aquatic Environment: A Review*; Elsevier: Amsterdam, The Netherlands, 1986.

116. Zaki, M.; Zakaria, A.; Eissa, I.A.E.; Eldeen, A. Effect of cadmium toxicity on Vertebrates. *Electron. Physician* **2016**, *8*, 1964–1965. [CrossRef]
117. Wyszowska, J.; Kucharski, J.; Kucharski, M.; Borowik, A. Effect of cadmium, copper and zinc on plants, soil microorganisms and soil enzymes. *J. Elementol.* **2012**, *18*, 769–796. [CrossRef]
118. Haider, F.U.; Liqun, C.; Coulter, J.A.; Cheema, S.A.; Wu, J.; Zhang, R.; Wenjun, M.; Farooq, M. Cadmium toxicity in plants: Impacts and remediation strategies. *Ecotoxicol. Environ. Saf.* **2021**, *211*, 111887. [CrossRef] [PubMed]
119. Ao, M.; Chen, X.; Deng, T.; Sun, S.; Tang, Y.; Morel, J.L.; Qiu, R.; Wang, S. Chromium biogeochemical behaviour in soil-plant systems and remediation strategies: A critical review. *J. Hazard. Mater.* **2022**, *424*, 127233. [CrossRef] [PubMed]
120. Sharma, A.; Kapoor, D.; Wang, J.; Shahzad, B.; Kumar, V.; Bali, A.S.; Jasrotia, S.; Zheng, B.; Yuan, H.; Yan, D. Chromium Bioaccumulation and Its Impacts on Plants: An Overview. *Plants* **2020**, *9*, 100. [CrossRef] [PubMed]
121. Regenspurg, S.; Geigenmüller, I.; Milsch, H.; Kühn, M. Copper precipitation as consequence of steel corrosion in a flow-through experiment mimicking a geothermal production well. *Geotherm. Energy* **2017**, *5*, 11. [CrossRef]
122. Mir, A.R.; Pichtel, J.; Hayat, S. Copper: Uptake, toxicity and tolerance in plants and management of Cu-contaminated soil. *Biomaterials* **2021**, *34*, 737–759. [CrossRef]
123. Htwe, T.; Onthong, J.; Duangpan, S.; Techato, K.; Chotikarn, P.; Sinutok, S. Effect of Copper Contamination on Plant Growth and Metal Contents in Rice Plant (*Oryza sativa* L.). *Commun. Soil. Sci. Plant Anal.* **2020**, *51*, 2349–2360. [CrossRef]
124. Kazmierczak, J.; Marty, N.; Holmslykke, H.D.; Weibel, R. *The Risk of Scaling and Corrosion Predicted Formation Water Composition for Danish Geothermal Plants*; Danish Energy Agency: Copenhagen, Denmark, 2019; p. 54.
125. Brown, K.; Lichti, K. Some current challenges in production geochemistry. In Proceedings of the New Zealand Geothermal Workshop, Auckland, New Zealand, 14–16 November 2022.
126. Miskimins, J.L. *Hydraulic Fracturing: Fundamentals and Advancements*; Society of Petroleum Engineers: Richardson, TX, USA, 2019. [CrossRef]
127. Gordalla, B.C.; Ewers, U.; Frimmel, F.H. Hydraulic fracturing: A toxicological threat for groundwater and drinking-water? *Environ. Earth Sci.* **2013**, *70*, 3875–3893. [CrossRef]
128. Wetherbee, O.; Meeker, J.R.; DeVoto, C.; Penning, T.M.; Moore, J.H.; Boland, M.R. WellExplorer: An integrative resource linking hydraulic fracturing chemicals with hormonal pathways and geographic location. *Database* **2020**, *2020*, baaa053. [CrossRef]
129. Chesnaux, R. A Tenth of Active and Abandoned Oil and Gas Wells in Northeastern B.C. are Leaking. Available online: <https://theconversation.com/a-tenth-of-active-and-abandoned-oil-and-gas-wells-in-northeastern-b-c-are-leaking-127921> (accessed on 18 September 2024).
130. Aminzadeh, F. *Hydraulic Fracturing and Well Stimulation*; John Wiley & Sons: Hoboken, NJ, USA, 2019. [CrossRef]
131. Dakheel Almaliki, A.J.; Bashir, M.J.K.; Llamas Borrajo, J.F. Appraisal of groundwater contamination from surface spills of fluids associated with hydraulic fracturing operations. *Sci. Total Environ.* **2022**, *815*, 152949. [CrossRef]
132. Sun, Y.; Wang, D.; Tsang, D.C.W.; Wang, L.; Ok, Y.S.; Feng, Y. A critical review of risks, characteristics, and treatment strategies for potentially toxic elements in wastewater from shale gas extraction. *Environ. Int.* **2019**, *125*, 452–469. [CrossRef]
133. Olsson, O.; Weichgrebe, D.; Rosenwinkel, K.-H. Hydraulic fracturing wastewater in Germany: Composition, treatment, concerns. *Environ. Earth Sci.* **2013**, *70*, 3895–3906. [CrossRef]
134. Knapik, E.; Chruszcz-Lipska, K.; Łukański, Ł.; Wysocki, S. Reuse of Flowback Water from Hydraulic Fracturing for Drilling Mud Preparation and Secondary Hydrocarbon Recovery. *Energies* **2021**, *14*, 5921. [CrossRef]
135. LAWA. *Determination of Insignificance Thresholds for Groundwater*; Länderarbeitsgemeinschaft Wasser (LAWA): Berlin, Germany, 2004.
136. Rosales, E.; Mejjide, J.; Pazos, M.; Sanroman, M.A. Challenges and recent advances in biochar as low-cost biosorbent: From batch assays to continuous-flow systems. *Bioresour. Technol.* **2017**, *246*, 176–192. [CrossRef] [PubMed]
137. Arif, M.; Liu, G.; Yousaf, B.; Ahmed, R.; Irshad, S.; Ashraf, A.; Zia-ur-Rehman, M.; Rashid, M.S. Synthesis, characteristics and mechanistic insight into the clays and clay minerals-biochar surface interactions for contaminants removal—A review. *J. Clean. Prod.* **2021**, *310*, 127548. [CrossRef]
138. Deng, J.; Liu, Y.; Li, H.; Huang, Z.; Qin, X.; Huang, J.; Zhang, X.; Li, X.; Lu, Q. A novel biochar-copolymer composite for rapid Cr(VI) removal: Adsorption-reduction performance and mechanism. *Sep. Purif. Technol.* **2022**, *295*, 121275. [CrossRef]
139. Ye, S.; Tan, X.; Yang, H.; Xiong, J.; Zhu, H.; Song, H.; Chen, G. Catalytic removal of attached tetrabromobisphenol A from microplastic surface by biochar activating oxidation and its impact on potential of disinfection by-products formation. *Water Res.* **2022**, *225*, 119191. [CrossRef]
140. Malyan, S.K.; Kumar, S.S.; Fagodiya, R.K.; Ghosh, P.; Kumar, A.; Singh, R.; Singh, L. Biochar for environmental sustainability in the energy-water-agroecosystem nexus. *Renew. Sustain. Energy Rev.* **2021**, *149*, 111379. [CrossRef]
141. Wang, Y.; Li, H.; Lin, S. Advances in the Study of Heavy Metal Adsorption from Water and Soil by Modified Biochar. *Water* **2022**, *14*, 3894. [CrossRef]
142. Bongosia, J.G.; Al-Gailani, A.; Kolosz, B.W.; Loy Chun Minh, A.; Lock, S.S.M.; Cheah, K.W.; Taylor, M.J. Scalable mesoporous biochars from bagasse waste for Cu (II) removal: Process optimisation, kinetics and techno-economic analysis. *J. Environ. Manag.* **2024**, *370*, 122558. [CrossRef]

143. Ambaye, T.G.; Vaccari, M.; van Hullebusch, E.D.; Amrane, A.; Rtimi, S. Mechanisms and adsorption capacities of biochar for the removal of organic and inorganic pollutants from industrial wastewater. *Int. J. Environ. Sci. Technol.* **2020**, *18*, 3273–3294. [\[CrossRef\]](#)
144. Abbas, Z.; Ali, S.; Rizwan, M.; Zaheer, I.E.; Malik, A.; Riaz, M.A.; Shahid, M.R.; Rehman, M.Z.u.; Al-Wabel, M.I. A critical review of mechanisms involved in the adsorption of organic and inorganic contaminants through biochar. *Arab. J. Geosci.* **2018**, *11*, 1–23. [\[CrossRef\]](#)
145. Masebinu, S.O.; Akinlabi, E.T.; Muzenda, E.; Aboyade, A.O. A review of biochar properties and their roles in mitigating challenges with anaerobic digestion. *Renew. Sustain. Energy Rev.* **2019**, *103*, 291–307. [\[CrossRef\]](#)
146. Wang, S.; Gao, B.; Zimmerman, A.R.; Li, Y.; Ma, L.; Harris, W.G.; Migliaccio, K.W. Removal of arsenic by magnetic biochar prepared from pinewood and natural hematite. *Bioresour. Technol.* **2015**, *175*, 391–395. [\[CrossRef\]](#) [\[PubMed\]](#)
147. Yang, X.; Zhang, S.; Ju, M.; Liu, L. Preparation and Modification of Biochar Materials and their Application in Soil Remediation. *Appl. Sci.* **2019**, *9*, 1365. [\[CrossRef\]](#)
148. Amusat, S.O.; Kebede, T.G.; Dube, S.; Nindi, M.M. Ball-milling synthesis of biochar and biochar-based nanocomposites and prospects for removal of emerging contaminants: A review. *J. Water Process Eng.* **2021**, *41*, 101993. [\[CrossRef\]](#)
149. Trakal, L.; Veselska, V.; Safarik, I.; Vitkova, M.; Cihlova, S.; Komarek, M. Lead and cadmium sorption mechanisms on magnetically modified biochars. *Bioresour. Technol.* **2016**, *203*, 318–324. [\[CrossRef\]](#)
150. Fang, F.; Liu, S.; Yuan, W.; Xiong, X.; Wang, J.; Qi, J.; Shi, Y.; Xu, W.; Liu, J.; Xiao, T. Superior removal of Tl(I) from aqueous solution by facilely engineered Mn_xO_y@potassium-rich biowaste-biochar. *Sep. Purif. Technol.* **2023**, *312*, 123294. [\[CrossRef\]](#)
151. Cairns, S.; Chaudhuri, S.; Sigmund, G.; Robertson, I.; Hawkins, N.; Dunlop, T.; Hofmann, T. Wood ash amended biochar for the removal of lead, copper, zinc and cadmium from aqueous solution. *Environ. Technol. Innov.* **2021**, *24*, 101961. [\[CrossRef\]](#)
152. Chen, T.; Zhou, Z.; Xu, S.; Wang, H.; Lu, W. Adsorption behavior comparison of trivalent and hexavalent chromium on biochar derived from municipal sludge. *Bioresour. Technol.* **2015**, *190*, 388–394. [\[CrossRef\]](#) [\[PubMed\]](#)
153. Uchimiya, M.; Bannon, D.I.; Wartelle, L.H.; Lima, I.M.; Klasson, K.T. Lead retention by broiler litter biochars in small arms range soil: Impact of pyrolysis temperature. *J. Agric. Food Chem.* **2012**, *60*, 5035–5044. [\[CrossRef\]](#)
154. Qiu, B.; Tao, X.; Wang, H.; Li, W.; Ding, X.; Chu, H. Biochar as a low-cost adsorbent for aqueous heavy metal removal: A review. *J. Anal. Appl. Pyrolysis* **2021**, *155*, 105081. [\[CrossRef\]](#)
155. Liu, Y.; Chen, Y.; Li, Y.; Chen, L.; Jiang, H.; Li, H.; Luo, X.; Tang, P.; Yan, H.; Zhao, M.; et al. Fabrication, application, and mechanism of metal and heteroatom co-doped biochar composites (MHBCs) for the removal of contaminants in water: A review. *J. Hazard. Mater.* **2022**, *431*, 128584. [\[CrossRef\]](#)
156. Zhang, C.; Lu, J.; Wu, J. One-step green preparation of magnetic seaweed biochar/sulfidated Fe(0) composite with strengthen adsorptive removal of tetrabromobisphenol A through in situ reduction. *Bioresour. Technol.* **2020**, *307*, 123170. [\[CrossRef\]](#) [\[PubMed\]](#)
157. Qiu, Y.; Cheng, H.; Xu, C.; Sheng, G.D. Surface characteristics of crop-residue-derived black carbon and lead(II) adsorption. *Water Res.* **2008**, *42*, 567–574. [\[CrossRef\]](#) [\[PubMed\]](#)
158. Qian, L.; Chen, M.; Chen, B. Competitive adsorption of cadmium and aluminum onto fresh and oxidized biochars during aging processes. *J. Soils Sediments* **2015**, *15*, 1130–1138. [\[CrossRef\]](#)
159. Zhang, A.; Li, X.; Xing, J.; Xu, G. Adsorption of potentially toxic elements in water by modified biochar: A review. *J. Environ. Chem. Eng.* **2020**, *8*, 104196. [\[CrossRef\]](#)
160. Premarathna, K.S.D.; Rajapaksha, A.U.; Sarkar, B.; Kwon, E.E.; Bhatnagar, A.; Ok, Y.S.; Vithanage, M. Biochar-based engineered composites for sorptive decontamination of water: A review. *Chem. Eng. J.* **2019**, *372*, 536–550. [\[CrossRef\]](#)
161. Qiu, B.; Shao, Q.; Shi, J.; Yang, C.; Chu, H. Application of biochar for the adsorption of organic pollutants from wastewater: Modification strategies, mechanisms and challenges. *Sep. Purif. Technol.* **2022**, *300*, 121925. [\[CrossRef\]](#)
162. Liu, B.L.; Fu, M.M.; Xiang, L.; Feng, N.X.; Zhao, H.M.; Li, Y.W.; Cai, Q.Y.; Li, H.; Mo, C.H.; Wong, M.H. Adsorption of microcystin contaminants by biochars derived from contrasting pyrolytic conditions: Characteristics, affecting factors, and mechanisms. *Sci. Total Environ.* **2021**, *763*, 143028. [\[CrossRef\]](#)
163. Zhang, H.; Song, X.; Zhang, J.; Liu, Y.; Hu, J.; Zhao, J. Performance and mechanism of Sycamore Flock based biochar in removing oxytetracycline hydrochloride. *Bioresour. Technol.* **2022**, *350*, 126884. [\[CrossRef\]](#)
164. Sun, K.; Ro, K.; Guo, M.; Novak, J.; Mashayekhi, H.; Xing, B. Sorption of bisphenol A, 17 α -ethinyl estradiol and phenanthrene on thermally and hydrothermally produced biochars. *Bioresour. Technol.* **2011**, *102*, 5757–5763. [\[CrossRef\]](#) [\[PubMed\]](#)
165. Inyang, M.; Dickenson, E. The potential role of biochar in the removal of organic and microbial contaminants from potable and reuse water: A review. *Chemosphere* **2015**, *134*, 232–240. [\[CrossRef\]](#) [\[PubMed\]](#)
166. Ni, J.; Pignatello, J.J.; Xing, B. Adsorption of aromatic carboxylate ions to black carbon (biochar) is accompanied by proton exchange with water. *Environ. Sci. Technol.* **2011**, *45*, 9240–9248. [\[CrossRef\]](#)
167. Jin, J.; Sun, K.; Wu, F.; Gao, B.; Wang, Z.; Kang, M.; Bai, Y.; Zhao, Y.; Liu, X.; Xing, B. Single-solute and bi-solute sorption of phenanthrene and dibutyl phthalate by plant- and manure-derived biochars. *Sci. Total Environ.* **2014**, *473*, 308–316. [\[CrossRef\]](#)
168. Gholizadeh, M.; Hu, X. Removal of heavy metals from soil with biochar composite: A critical review of the mechanism. *J. Environ. Chem. Eng.* **2021**, *9*, 105830. [\[CrossRef\]](#)
169. Cao, X.; Harris, W. Properties of dairy-manure-derived biochar pertinent to its potential use in remediation. *Bioresour. Technol.* **2010**, *101*, 5222–5228. [\[CrossRef\]](#)

170. Chen, H.; Yuan, X.; Xiong, T.; Jiang, L.; Wang, H.; Wu, Z. Biochar Facilitated Hydroxyapatite/Calcium Silicate Hydrate for Remediation of Heavy Metals Contaminated Soils. *Water Air Soil Pollut.* **2020**, *231*, 66. [\[CrossRef\]](#)
171. Inyang, M.; Gao, B.; Ding, W.; Pullammanappallil, P.; Zimmerman, A.R.; Cao, X. Enhanced Lead Sorption by Biochar Derived from Anaerobically Digested Sugarcane Bagasse. *Sep. Sci. Technol.* **2011**, *46*, 1950–1956. [\[CrossRef\]](#)
172. Su, X.; Chen, Y.; Li, Y.; Li, J.; Song, W.; Li, X.; Yan, L. Enhanced adsorption of aqueous Pb(II) and Cu(II) by biochar loaded with layered double hydroxide: Crucial role of mineral precipitation. *J. Mol. Liq.* **2022**, *357*, 119083. [\[CrossRef\]](#)
173. Rizwan, M.; Ali, S.; Qayyum, M.F.; Ibrahim, M.; Zia-ur-Rehman, M.; Abbas, T.; Ok, Y.S. Mechanisms of biochar-mediated alleviation of toxicity of trace elements in plants: A critical review. *Environ. Sci. Pollut. Res. Int.* **2016**, *23*, 2230–2248. [\[CrossRef\]](#)
174. Inyang, M.I.; Gao, B.; Yao, Y.; Xue, Y.; Zimmerman, A.; Mosa, A.; Pullammanappallil, P.; Ok, Y.S.; Cao, X. A review of biochar as a low-cost adsorbent for aqueous heavy metal removal. *Crit. Rev. Environ. Sci. Technol.* **2016**, *46*, 406–433. [\[CrossRef\]](#)
175. Liu, L.; Yang, X.; Ahmad, S.; Li, X.; Ri, C.; Tang, J.; Ellam, R.M.; Song, Z. Silicon (Si) modification of biochars from different Si-bearing precursors improves cadmium remediation. *Chem. Eng. J.* **2023**, *457*, 141194. [\[CrossRef\]](#)
176. Mishra, V.; Sureshkumar, M.K.; Gupta, N.; Kaushik, C.P. Study on Sorption Characteristics of Uranium onto Biochar Derived from Eucalyptus Wood. *Water Air Soil. Pollut.* **2017**, *228*, 309. [\[CrossRef\]](#)
177. Sen Gupta, S.; Bhattacharyya, K.G. Kinetics of adsorption of metal ions on Inorganic Materials: A Review. *Adv. Colloid. Interface Sci.* **2011**, *162*, 39–58. [\[CrossRef\]](#)
178. Gupta, S.; Sireesha, S.; Sreedhar, I.; Patel, C.M.; Anitha, K.L. Latest trends in heavy metal removal from wastewater by biochar based sorbents. *J. Water Process Eng.* **2020**, *38*, 101561. [\[CrossRef\]](#)
179. Abdi, O.; Kazemi, M. A review study of biosorption of heavy metals and comparison between different biosorbents. *J. Mater. Environ. Sci.* **2015**, *6*, 1386–1399.
180. Tan, K.L.; Hameed, B.H. Insight into the adsorption kinetics models for the removal of contaminants from aqueous solutions. *J. Taiwan. Inst. Chem. Eng.* **2017**, *74*, 25–48. [\[CrossRef\]](#)
181. Chinoune, K.; Bentaleb, K.; Bouberka, Z.; Nadim, A.; Maschke, U. Adsorption of reactive dyes from aqueous solution by Dirty Bentonite. *Appl. Clay Sci.* **2016**, *123*, 64–75. [\[CrossRef\]](#)
182. Yousef, R.I.; El-Eswed, B.; Al-Muhtaseb, A.A.H. Adsorption characteristics of natural zeolites as solid adsorbents for phenol removal from aqueous solutions: Kinetics, mechanism, and thermodynamics studies. *Chem. Eng. J.* **2011**, *171*, 1143–1149. [\[CrossRef\]](#)
183. Ho, Y.S.; McKay, G. Pseudo-second order model for Sorption Processes. *Process Biochem.* **1999**, *34*, 451–465. [\[CrossRef\]](#)
184. Setiabudi, H.D.; Jusoh, R.; Suhaimi, S.F.R.M.; Masrur, S.F. Adsorption of methylene blue onto oil palm (*Elaeis guineensis*) leaves: Process optimization, isotherm, kinetics and thermodynamic studies. *J. Taiwan Inst. Chem. Eng.* **2016**, *63*, 363–370. [\[CrossRef\]](#)
185. Allen, S.J.; Gan, Q.; Matthews, R.; Johnson, P.A. Kinetic modeling of the adsorption of basic dyes by kudzu. *J. Colloid Interface Sci.* **2005**, *286*, 101–109. [\[CrossRef\]](#) [\[PubMed\]](#)
186. Hu, S.; Liu, C.; Bu, H.; Chen, M.; Fei, Y.-h. Efficient reduction and adsorption of Cr(VI) using FeCl₃-modified biochar: Synergistic roles of persistent free radicals and Fe(II). *J. Environ. Sci.* **2024**, *137*, 626–638. [\[CrossRef\]](#) [\[PubMed\]](#)
187. Yoon, K.; Cho, D.-W.; Kwon, G.; Rinklebe, J.; Wang, H.; Song, H. Practical approach of As(V) adsorption by fabricating biochar with low basicity from FeCl₃ and lignin. *Chemosphere* **2023**, *329*, 138665. [\[CrossRef\]](#) [\[PubMed\]](#)
188. Zhang, D.; Zhou, D.; Lu, L.; Zhang, M.; Lü, T.; Huang, J.; Zhao, H.; Zhou, J.; Rinklebe, J. Preferential, synergistic sorption and reduction of cr(vi) from Chromium–Rhodamine B mixed wastewater by magnetic porous biochar derived from wasted *Myriophyllum aquaticum* biomass. *Environ. Pollut.* **2023**, *327*, 121593. [\[CrossRef\]](#)
189. Zhang, W.-X.; Chen, X.; Xiao, G.-S.; Liang, J.-Y.; Kong, L.-J.; Yao, X.-W.; Diao, Z.-H. A novel pigeon waste based biochar composite for the removal of heavy metal and organic compound: Performance, products and mechanism. *Colloids Surf. A Physicochem. Eng. Asp.* **2023**, *666*, 131277. [\[CrossRef\]](#)
190. Fan, S.; Fan, X.; Wang, S.; Li, B.; Zhou, N.; Xu, H. Effect of chitosan modification on the properties of magnetic porous biochar and its adsorption performance towards tetracycline and cu²⁺. *Sustain. Chem. Pharm.* **2023**, *33*, 101057. [\[CrossRef\]](#)
191. Li, X.; Liu, T.; Han, X.; Li, Y.; Ma, X. Removal of heavy metals lead and ciprofloxacin from farm wastewater using Peanut Shell biochar. *Environ. Technol. Innov.* **2023**, *30*, 103121. [\[CrossRef\]](#)
192. Kamran, U.; Lee, S.-Y.; Rhee, K.Y.; Park, S.-J. Rice husk valorization into sustainable Ni@TiO₂/biochar nanocomposite for highly selective Pb (ii) ions removal from an aqueous media. *Chemosphere* **2023**, *323*, 138210. [\[CrossRef\]](#)
193. Johnson, V.E.; Liao, Q.; Jallawide, B.W.; Anaman, R.; Amanze, C.; Huang, P.; Cao, W.; Ding, C.; Shi, Y. Simultaneous removal of as(v) and pb(ii) using highly-efficient modified dehydrated biochar made from banana peel via hydrothermal synthesis. *Colloids Surf. A Physicochem. Eng. Asp.* **2023**, *663*, 131115. [\[CrossRef\]](#)
194. Yao, B.; Li, Y.; Zeng, W.; Yang, G.; Zeng, J.; Nie, J.; Zhou, Y. Synergistic adsorption and oxidation of trivalent antimony from groundwater using biochar supported magnesium ferrite: Performances and mechanisms. *Environ. Pollut.* **2023**, *323*, 121318. [\[CrossRef\]](#)
195. Zong, Y.; Wang, X.; Zhang, H.; Li, Y.; Yu, J.; Wang, C.; Cai, Z.; Wei, J.; Ding, L. Preparation of a ternary composite based on water caltrop shell derived biochar and gelatin/alginate for cadmium removal from contaminated water: Performances assessment and mechanism insight. *Int. J. Biol. Macromol.* **2023**, *234*, 123637. [\[CrossRef\]](#) [\[PubMed\]](#)
196. Chen, G.; Wang, H.; Han, L.; Yang, N.; Hu, B.; Qiu, M.; Zhong, X. Highly efficient removal of U(VI) by a novel biochar supported with fes nanoparticles and chitosan composites. *J. Mol. Liq.* **2021**, *327*, 114807. [\[CrossRef\]](#)

197. Siddiqui, S.; Bhatnagar, P.; Sireesha, S.; Sopanrao, K.S.; Sreedhar, I. Efficient copper removal using low-cost H_3PO_4 impregnated Red-Gram Biochar-MnO₂ nanocomposites. *Bioresour. Technol. Rep.* **2023**, *21*, 101304. [\[CrossRef\]](#)
198. Qi, G.; Pan, Z.; Zhang, X.; Chang, S.; Wang, H.; Wang, M.; Xiang, W.; Gao, B. Microwave biochar produced with activated carbon catalyst: Characterization and adsorption of heavy metals. *Environ. Res.* **2023**, *216*, 114732. [\[CrossRef\]](#)
199. Zhou, D.; Xie, G.; Hu, X.; Cai, X.; Zhao, Y.; Hu, X.; Jin, Q.; Fu, X.; Tan, X.; Liang, C.; et al. Coupling of kenaf biochar and magnetic BIFEO₃ onto cross-linked chitosan for enhancing separation performance and Cr(VI) ions removal efficiency. *Int. J. Environ. Res. Public Health* **2020**, *17*, 788. [\[CrossRef\]](#)
200. Qin, L.; He, L.; Yang, W.; Lin, A. Preparation of a novel iron-based biochar composite for removal of hexavalent chromium in water. *Environ. Sci. Pollut. Res.* **2020**, *27*, 9214–9226. [\[CrossRef\]](#)
201. Xiao, F.e.a. Removal of heavy metals from aqueous solution using chitosan-combined magnetic biochars. *J. Colloid Interface Sci.* **2019**, *540*, 579–584. [\[CrossRef\]](#)
202. Chen, H.; Guo, H.; Jiang, D.; Cheng, S.; Xing, B.; Meng, W.; Fang, J.; Xia, H. Microwave-assisted pyrolysis of rape stalk to prepare biochar for heavy metal wastewater removal. *Diam. Relat. Mater.* **2023**, *134*, 109794. [\[CrossRef\]](#)
203. Herath, A.; Layne, C.A.; Perez, F.; Hassan, E.I.B.; Pittman, C.U.; Mlsna, T.E. Koh-activated high surface area Douglas Fir Biochar for adsorbing aqueous Cr(VI), Pb(II) and Cd(II). *Chemosphere* **2021**, *269*, 128409. [\[CrossRef\]](#)
204. Zhang, X.; Wang, H.; He, L.; Lu, K.; Sarmah, A.; Li, J.-W.; Bolan, N.; Pei, J.; Huang, H. Using biochar for remediation of soils contaminated with heavy metals and organic pollutants. *Environ. Sci. Pollut. Res.* **2013**, *20*, 8472–8483. [\[CrossRef\]](#) [\[PubMed\]](#)
205. Chen, Z.; Xiao, X.; Xing, B.; Chen, B. pH-dependent sorption of sulfonamide antibiotics onto biochars: Sorption mechanisms and modeling. *Environ. Pollut.* **2019**, *248*, 48–56. [\[CrossRef\]](#) [\[PubMed\]](#)
206. Gao, Z.; Shan, D.; He, J.; Huang, T.; Mao, Y.; Tan, H.; Shi, H.; Li, T.; Xie, T. Effects and mechanism on cadmium adsorption removal by CaCl₂-modified biochar from selenium-rich straw. *Bioresour. Technol.* **2023**, *370*, 128563. [\[CrossRef\]](#) [\[PubMed\]](#)
207. Yan, S.; Yu, W.; Yang, T.; Li, Q.; Guo, J. The adsorption of corn stalk biochar for Pb and Cd: Preparation, characterization, and batch adsorption study. *Separations* **2022**, *9*, 22. [\[CrossRef\]](#)
208. Sakhiya, A.K.; Vijay, V.K.; Kaushal, P. Efficacy of rice straw derived biochar for removal of Pb²⁺ and Zn²⁺ from aqueous: Adsorption, thermodynamic and cost analysis. *Bioresour. Technol. Rep.* **2022**, *17*, 100920. [\[CrossRef\]](#)
209. Li, Y.; Du, Q.; Wang, X.; Zhang, P.; Wang, D.; Wang, Z.; Xia, Y. Removal of lead from aqueous solution by activated carbon prepared from enteromorpha prolifera by zinc chloride activation. *J. Hazard. Mater.* **2010**, *183*, 583–589. [\[CrossRef\]](#)
210. Hakeem, I.G.; Halder, P.; Marzbali, M.H.; Patel, S.; Rathnayake, N.; Surapaneni, A.; Short, G.; Paz-Ferreiro, J.; Shah, K. Mild sulphuric acid pre-treatment for metals removal from biosolids and the fate of metals in the treated biosolids derived biochar. *J. Environ. Chem. Eng.* **2022**, *10*, 107378. [\[CrossRef\]](#)
211. Arán, D.; Antelo, J.; Lodeiro, P.; Macías, F.; Fiol, S. Use of Waste-Derived Biochar to Remove Copper from Aqueous Solution in a Continuous-Flow System. *Ind. Eng. Chem. Res.* **2017**, *56*, 12755–12762. [\[CrossRef\]](#)
212. Asadullah; Kaewsichan, L.; Techato, K.; Qaisrani, Z.N.; Chowdhury, M.S.; Yilmaz, M. Elimination of selected heavy metals from aqueous solutions using biochar and bentonite composite monolith in a fixed-bed operation. *J. Environ. Chem. Eng.* **2022**, *10*, 106993. [\[CrossRef\]](#)
213. Ajala, O.A.; Akinlawo, S.O.; Bamisaye, A.; Adedipe, D.T.; Adesina, M.O.; Okon-Akan, O.A.; Adebuseyi, T.A.; Ojedokun, A.T.; Adegoke, K.A.; Bello, O.S. Adsorptive removal of antibiotic pollutants from wastewater using biomass/biochar-based adsorbents. *RSC Adv.* **2023**, *13*, 4678–4712. [\[CrossRef\]](#)
214. Sutar, S.; Patil, P.; Jadhav, J. Recent advances in biochar technology for textile dyes wastewater remediation: A Review. *Environ. Res.* **2022**, *209*, 112841. [\[CrossRef\]](#) [\[PubMed\]](#)
215. Dai, Y.e.a. The adsorption, regeneration and engineering applications of Biochar for Removal Organic Pollutants: A Review. *Chemosphere* **2019**, *223*, 12–27. [\[CrossRef\]](#)
216. Greiner, B.G.; Shimabuku, K.K.; Summers, R.S. Influence of biochar thermal regeneration on sulfamethoxazole and dissolved organic matter adsorption. *Environ. Sci. Water Res. Technol.* **2018**, *4*, 169–174. [\[CrossRef\]](#)
217. Alsawy, T.; Rashad, E.; El-Qelish, M.; Mohammed, R.H. A comprehensive review on the chemical regeneration of biochar adsorbent for sustainable wastewater treatment. *npj Clean Water* **2022**, *5*, 29. [\[CrossRef\]](#)
218. Wang, S.-y.; Tang, Y.-k.; Chen, C.; Wu, J.-t.; Huang, Z.; Mo, Y.-y.; Zhang, K.-x.; Chen, J.-b. Regeneration of magnetic biochar derived from eucalyptus leaf residue for lead(II) removal. *Bioresour. Technol.* **2015**, *186*, 360–364. [\[CrossRef\]](#) [\[PubMed\]](#)
219. Jia, Y.; Zhang, Y.; Fu, J.; Yuan, L.; Li, Z.; Liu, C.; Zhao, D.; Wang, X. A novel magnetic biochar/MgFe-layered double hydroxides composite removing Pb²⁺ from aqueous solution: Isotherms, kinetics and thermodynamics. *Colloids Surf. A Physicochem. Eng. Asp.* **2019**, *567*, 278–287. [\[CrossRef\]](#)
220. Wu, Z.; Chen, X.; Yuan, B.; Fu, M.-L. A facile foaming-polymerization strategy to prepare 3D MnO₂ modified biochar-based porous hydrogels for efficient removal of Cd(II) and Pb(II). *Chemosphere* **2020**, *239*, 124745. [\[CrossRef\]](#)
221. Zubrik, A.; Matik, M.; Mačingová, E.; Danková, Z.; Jáger, D.; Briančin, J.; Machala, L.; Pechoušek, J.; Hredzák, S. The use of microwave irradiation for preparation and fast-acting regeneration of magnetic biochars. *Chem. Eng. Process.-Process Intensif.* **2022**, *178*, 109016. [\[CrossRef\]](#)
222. Oladejo, J.; Shi, K.; Chen, Y.; Luo, X.; Gang, Y.; Wu, T. Closing the active carbon cycle: Regeneration of spent activated carbon from a wastewater treatment facility for resource optimization. *Chem. Eng. Process.-Process Intensif.* **2020**, *150*, 107878. [\[CrossRef\]](#)

223. Kumar, A.; Singh, E.; Mishra, R.; Lo, S.-L.; Kumar, S. A green approach towards sorption of CO₂ on waste derived biochar. *Environ. Res.* **2022**, *214*, 113954. [\[CrossRef\]](#)
224. Liao, Y.; Jiang, L.; Cao, X.; Zheng, H.; Feng, L.; Mao, Y.; Zhang, Q.; Shen, Q.; Ji, F. Efficient removal mechanism and microbial characteristics of tidal flow constructed wetland based on in-situ biochar regeneration (BR-TFCW) for Rural Gray Water. *Chem. Eng. J.* **2022**, *431*, 134185. [\[CrossRef\]](#)
225. Faheem; Du, J.; Kim, S.H.; Hassan, M.A.; Irshad, S.; Bao, J. Application of biochar in advanced oxidation processes: Supportive, adsorptive, and catalytic role. *Environ. Sci. Pollut. Res.* **2020**, *27*, 37286–37312. [\[CrossRef\]](#) [\[PubMed\]](#)
226. Yameen, M.Z.; Naqvi, S.R.; Juchelková, D.; Khan, M.N.A. Harnessing the power of functionalized biochar: Progress, challenges, and future perspectives in energy, water treatment, and environmental sustainability. *Biochar* **2024**, *6*, 25. [\[CrossRef\]](#)
227. Gao, N.; Du, W.; Zhang, M.; Ling, G.; Zhang, P. Chitosan-modified biochar: Preparation, modifications, mechanisms and applications. *Int. J. Biol. Macromol.* **2022**, *209*, 31–49. [\[CrossRef\]](#) [\[PubMed\]](#)
228. Loc, N.X.; Tuyen, P.T.; Mai, L.C.; Phuong, D.T. Chitosan-Modified Biochar and Unmodified Biochar for Methyl Orange: Adsorption Characteristics and Mechanism Exploration. *Toxics* **2022**, *10*, 500. [\[CrossRef\]](#)
229. Hussain, A.; Maitra, J.; Khan, K.A. Development of biochar and chitosan blend for heavy metals uptake from synthetic and industrial wastewater. *Appl. Water Sci.* **2017**, *7*, 4525–4537. [\[CrossRef\]](#)
230. Ainscough, T.J.; Alagappan, P.; Oatley-Radcliffe, D.L.; Barron, A.R. A hybrid super hydrophilic ceramic membrane and carbon nanotube adsorption process for clean water production and heavy metal removal and recovery in remote locations. *J. Water Process Eng.* **2017**, *19*, 220–230. [\[CrossRef\]](#)
231. Mulyati, S.; Syawaliah, S. Removal of Cd₂₊ and Pb²⁺ heavy metals in water by using adsorption-ultrafiltration hybrid process. *J. Teknol.* **2018**, *80*, 17–22. [\[CrossRef\]](#)
232. Çermikli, E.; Şen, F.; Altıok, E.; Wolska, J.; Cyganowski, P.; Kabay, N.; Bryjak, M.; Arda, M.; Yüksel, M. Performances of novel chelating ion exchange resins for boron and arsenic removal from saline geothermal water using adsorption-membrane filtration hybrid process. *Desalination* **2020**, *491*, 114504. [\[CrossRef\]](#)
233. Song, B.; Cao, X.; Gao, W.; Aziz, S.; Gao, S.; Lam, C.-H.; Lin, R. Preparation of nano-biochar from conventional biorefineries for high-value applications. *Renew. Sustain. Energy Rev.* **2022**, *157*, 112057. [\[CrossRef\]](#)
234. Chausali, N.; Saxena, J.; Prasad, R. Nanobiochar and biochar based nanocomposites: Advances and applications. *J. Agric. Food Res.* **2021**, *5*, 100191. [\[CrossRef\]](#)
235. Xiao, J.; Hu, R.; Chen, G. Micro-nano-engineered nitrogenous bone biochar developed with a ball-milling technique for high-efficiency removal of aquatic Cd(II), Cu(II) and Pb(II). *J. Hazard. Mater.* **2020**, *387*, 121980. [\[CrossRef\]](#) [\[PubMed\]](#)
236. Yu, F.; Tian, F.; Zou, H.; Ye, Z.; Peng, C.; Huang, J.; Zheng, Y.; Zhang, Y.; Yang, Y.; Wei, X.; et al. ZnO/biochar nanocomposites via solvent free ball milling for enhanced adsorption and photocatalytic degradation of methylene blue. *J. Hazard. Mater.* **2021**, *415*, 125511. [\[CrossRef\]](#) [\[PubMed\]](#)
237. Zhang, M.; Gao, B.; Yao, Y.; Xue, Y.; Inyang, M. Synthesis of porous MgO-biochar nanocomposites for removal of phosphate and nitrate from aqueous solutions. *Chem. Eng. J.* **2012**, *210*, 26–32. [\[CrossRef\]](#)
238. Hosny, M.; Fawzy, M.; Eltaweil, A.S. Phytofabrication of bimetallic silver-copper/biochar nanocomposite for environmental and medical applications. *J. Environ. Manag.* **2022**, *316*, 115238. [\[CrossRef\]](#)
239. Han, S.; Xiao, P. Catalytic degradation of tetracycline using peroxymonosulfate activated by cobalt and iron co-loaded pomelo peel biochar nanocomposite: Characterization, performance and reaction mechanism. *Sep. Purif. Technol.* **2022**, *287*, 120533. [\[CrossRef\]](#)
240. Wang, S.; Xiao, D.; Zheng, X.; Zheng, L.; Yang, Y.; Zhang, H.; Ai, B.; Sheng, Z. Halloysite and coconut shell biochar magnetic composites for the sorption of Pb(II) in wastewater: Synthesis, characterization and mechanism investigation. *J. Environ. Chem. Eng.* **2021**, *9*, 106865. [\[CrossRef\]](#)
241. Yap, M.W.; Mubarak, N.M.; Sahu, J.N.; Abdullah, E.C. Microwave induced synthesis of magnetic biochar from agricultural biomass for removal of lead and cadmium from wastewater. *J. Ind. Eng. Chem.* **2017**, *45*, 287–295. [\[CrossRef\]](#)
242. Han, Y.; Cao, X.; Ouyang, X.; Sohi, S.P.; Chen, J. Adsorption kinetics of magnetic biochar derived from peanut hull on removal of Cr (VI) from aqueous solution: Effects of production conditions and particle size. *Chemosphere* **2016**, *145*, 336–341. [\[CrossRef\]](#)
243. Hale, L.; Luth, M.; Crowley, D. Biochar characteristics relate to its utility as an alternative soil inoculum carrier to peat and vermiculite. *Soil. Biol. Biochem.* **2015**, *81*, 228–235. [\[CrossRef\]](#)
244. Frankel, M.L.; Bhuiyan, T.I.; Veksha, A.; Demeter, M.A.; Layzell, D.B.; Helleur, R.J.; Hill, J.M.; Turner, R.J. Removal and biodegradation of naphthenic acids by biochar and attached environmental biofilms in the presence of co-contaminating metals. *Bioresour. Technol.* **2016**, *216*, 352–361. [\[CrossRef\]](#) [\[PubMed\]](#)
245. McKenzie, N.; Yue, S.; Liu, X.; Ramsay, B.A.; Ramsay, J.A. Biodegradation of naphthenic acids in oils sands process waters in an immobilized soil/sediment bioreactor. *Chemosphere* **2014**, *109*, 164–172. [\[CrossRef\]](#) [\[PubMed\]](#)
246. Castro, C.; Urbiet, M.S.; Cazón, J.P.; Donati, E.R. Metal biorecovery and bioremediation: Whether or not thermophilic are better than mesophilic microorganisms. *Bioresour. Technol.* **2019**, *279*, 317–326. [\[CrossRef\]](#)
247. Kumar, M.; Yadav, A.N.; Saxena, R.; Paul, D.; Tomar, R.S. Biodiversity of pesticides degrading microbial communities and their environmental impact. *Biocatal. Agric. Biotechnol.* **2021**, *31*, 101883. [\[CrossRef\]](#)
248. Li, Y.; Xin, M.; Xie, D.; Fan, S.; Ma, J.; Liu, K.; Yu, F. Variation in extracellular polymeric substances from *Enterobacter* sp. and their Pb²⁺ adsorption behaviors. *ACS Omega* **2021**, *6*, 9617–9628. [\[CrossRef\]](#)

249. Manikandan, S.K.; Pallavi, P.; Shetty, K.; Bhattacharjee, D.; Giannakoudakis, D.A.; Katsoyiannis, I.A.; Nair, V. Effective Usage of Biochar and Microorganisms for the Removal of Heavy Metal Ions and Pesticides. *Molecules* **2023**, *28*, 719. [\[CrossRef\]](#)
250. Osman, A.I.; Fawzy, S.; Farghali, M.; El-Azazy, M.; Elgarahy, A.M.; Fahim, R.A.; Maksoud, M.I.A.A.; Ajlan, A.A.; Yousry, M.; Saleem, Y.; et al. Biochar for agronomy, animal farming, anaerobic digestion, composting, water treatment, soil remediation, construction, energy storage, and carbon sequestration: A review. *Environ. Chem. Lett.* **2022**, *20*, 2385–2485. [\[CrossRef\]](#) [\[PubMed\]](#)
251. Sun, T.; Miao, J.; Saleem, M.; Zhang, H.; Yang, Y.; Zhang, Q. Bacterial compatibility and immobilization with biochar improved tebuconazole degradation, soil microbiome composition and functioning. *J. Hazard. Mater.* **2020**, *398*, 122941. [\[CrossRef\]](#) [\[PubMed\]](#)
252. Teng, Z.; Shao, W.; Zhang, K.; Yu, F.; Huo, Y.; Li, M. Enhanced passivation of lead with immobilized phosphate solubilizing bacteria beads loaded with biochar/nanoscale zero valent iron composite. *J. Hazard. Mater.* **2020**, *384*, 121505. [\[CrossRef\]](#)
253. Wang, T.; Sun, H.; Ren, X.; Li, B.; Mao, H. Adsorption of heavy metals from aqueous solution by UV-mutant *Bacillus subtilis* loaded on biochars derived from different stock materials. *Ecotoxicol. Environ. Saf.* **2018**, *148*, 285–292. [\[CrossRef\]](#)
254. Chen, H.; Zhang, J.; Tang, L.; Su, M.; Tian, D.; Zhang, L.; Li, Z.; Hu, S. Enhanced Pb immobilization via the combination of biochar and phosphate solubilizing bacteria. *Environ. Int.* **2019**, *127*, 395–401. [\[CrossRef\]](#) [\[PubMed\]](#)
255. Shen, Y.; Li, H.; Zhu, W.; Ho, S.-H.; Yuan, W.; Chen, J.; Xie, Y. Microalgal-biochar immobilized complex: A novel efficient biosorbent for cadmium removal from aqueous solution. *Bioresour. Technol.* **2017**, *244*, 1031–1038. [\[CrossRef\]](#) [\[PubMed\]](#)
256. Huang, S.-W.; Chen, X.; Wang, D.-D.; Jia, H.-L.; Wu, L. Bio-reduction and synchronous removal of hexavalent chromium from aqueous solutions using novel microbial cell/algal-derived biochar particles: Turning an environmental problem into an opportunity. *Bioresour. Technol.* **2020**, *309*, 123304. [\[CrossRef\]](#) [\[PubMed\]](#)
257. Zhang, X.; Li, Y.; Li, H. Enhanced bio-immobilization of Pb contaminated soil by immobilized bacteria with biochar as carrier. *Pol. J. Environ. Stud.* **2017**, *26*, 413–418. [\[CrossRef\]](#)
258. Ma, H.; Wei, M.; Wang, Z.; Hou, S.; Li, X.; Xu, H. Bioremediation of cadmium polluted soil using a novel cadmium immobilizing plant growth promotion strain *Bacillus* sp. TZ5 loaded on biochar. *J. Hazard. Mater.* **2020**, *388*, 122065. [\[CrossRef\]](#)
259. Liu, Y.; Tie, B.; Peng, O.; Luo, H.; Li, D.; Liu, S.; Lei, M.; Wei, X.; Liu, X.; Du, H. Inoculation of Cd-contaminated paddy soil with biochar-supported microbial cell composite: A novel approach to reducing cadmium accumulation in rice grains. *Chemosphere* **2020**, *247*, 125850. [\[CrossRef\]](#)
260. Tu, C.; Wei, J.; Guan, F.; Liu, Y.; Sun, Y.; Luo, Y. Biochar and bacteria inoculated biochar enhanced Cd and Cu immobilization and enzymatic activity in a polluted soil. *Environ. Int.* **2020**, *137*, 105576. [\[CrossRef\]](#)
261. Youngwilai, A.; Kidkhunthod, P.; Jearanaikoon, N.; Chaiprapa, J.; Supanchaiyamat, N.; Hunt, A.J.; Ngernyen, Y.; Ratpukdi, T.; Khan, E.; Siripattanakul-Ratpukdi, S. Simultaneous manganese adsorption and biotransformation by *Streptomyces violaceus* strain SBP1 cell-immobilized biochar. *Sci. Total Environ.* **2020**, *713*, 136708. [\[CrossRef\]](#) [\[PubMed\]](#)
262. Manikandan, S.K.; Nair, V. *Pseudomonas stutzeri* Immobilized Sawdust Biochar for Nickel Ion Removal. *Catalysts* **2022**, *12*, 1495. [\[CrossRef\]](#)
263. Qi, X.; Gou, J.; Chen, X.; Xiao, S.; Ali, I.; Shang, R.; Wang, D.; Wu, Y.; Han, M.; Luo, X. Application of mixed bacteria-loaded biochar to enhance uranium and cadmium immobilization in a co-contaminated soil. *J. Hazard. Mater.* **2021**, *401*, 123823. [\[CrossRef\]](#)
264. Sajid, M.; Basheer, C. Stir-bar supported micro-solid-phase extraction for the determination of polychlorinated biphenyl congeners in serum samples. *J. Chromatogr. A* **2016**, *1455*, 37–44. [\[CrossRef\]](#) [\[PubMed\]](#)
265. Wang, S.; Gao, B.; Wan, Y.; Creamer, A. Sorption of arsenate onto magnetic iron-manganese (Fe-Mn) biochar composites. *RSC Adv.* **2015**, *5*, 67971–67978. [\[CrossRef\]](#)
266. Wang, S.; Gao, B.; Li, Y. Enhanced arsenic removal by biochar modified with nickel (Ni) and manganese (Mn) oxyhydroxides. *J. Ind. Eng. Chem.* **2016**, *37*, 361–365. [\[CrossRef\]](#)
267. Zubair, M.; Manzar, M.; El-Qanni, A.; Haroon, H.; Alqahtani, H.; Al-Ejji, M.; Mu'azu, N.; AlGhamdi, J.; Haladu, S.; Al-Hashim, D.; et al. Biochar-layered double hydroxide composites for the adsorption of tetracycline from water: Synthesis, process modeling, and mechanism. *Environ. Sci. Pollut. Res.* **2023**, *30*, 1–19. [\[CrossRef\]](#)
268. Qiu, M.; Liu, L.; Ling, Q.; Cai, Y.; Yu, S.; Wang, S.; Fu, D.; Hu, B.; Wang, X. Biochar for the removal of contaminants from soil and water: A review. *Biochar* **2022**, *4*, 19. [\[CrossRef\]](#)
269. dos Santos, G.E.d.S.; Lins, P.V.d.S.; Oliveira, L.M.T.d.M.; Silva, E.O.d.; Anastopoulos, I.; Erto, A.; Giannakoudakis, D.A.; Almeida, A.R.F.d.; Duarte, J.L.d.S.; Meili, L. Layered double hydroxides/biochar composites as adsorbents for water remediation applications: Recent trends and perspectives. *J. Clean. Prod.* **2021**, *284*, 124755. [\[CrossRef\]](#)
270. Singh, A.; Chaubey, A.; Kaur, I. Remediation of water contaminated with antibiotics using biochar modified with layered double hydroxide: Preparation and performance. *J. Hazard. Mater. Adv.* **2023**, *10*, 100286. [\[CrossRef\]](#)
271. Fang, Q.; Ye, S.; Yang, H.; Yang, K.; Zhou, J.; Gao, Y.; Lin, Q.; Tan, X.; Yang, Z. Application of layered double hydroxide-biochar composites in wastewater treatment: Recent trends, modification strategies, and outlook. *J. Hazard. Mater.* **2021**, *420*, 126569. [\[CrossRef\]](#)
272. Zubair, M.; Ihsanullah, I.; Abdul Aziz, H.; Azmier Ahmad, M.; Al-Harthi, M.A. Sustainable wastewater treatment by biochar/layered double hydroxide composites: Progress, challenges, and outlook. *Bioresour. Technol.* **2021**, *319*, 124128. [\[CrossRef\]](#) [\[PubMed\]](#)
273. Wan, S.; Wang, S.; Li, Y.; Gao, B. Functionalizing biochar with Mg–Al and Mg–Fe layered double hydroxides for removal of phosphate from aqueous solutions. *J. Ind. Eng. Chem.* **2017**, *47*, 246–253. [\[CrossRef\]](#)

274. Zhang, Z.; Yan, L.; Yu, H.; Yan, T.; Li, X. Adsorption of phosphate from aqueous solution by vegetable biochar/layered double oxides: Fast removal and mechanistic studies. *Bioresour. Technol.* **2019**, *284*, 65–71. [[CrossRef](#)] [[PubMed](#)]
275. Huang, D.; Liu, C.; Zhang, C.; Deng, R.; Wang, R.; Xue, W.; Luo, H.; Zeng, G.; Zhang, Q.; Guo, X. Cr(VI) removal from aqueous solution using biochar modified with Mg/Al-layered double hydroxide intercalated with ethylenediaminetetraacetic acid. *Bioresour. Technol.* **2019**, *276*, 127–132. [[CrossRef](#)] [[PubMed](#)]
276. Yang, F.; Zhang, S.; Sun, Y.; Tsang, D.C.W.; Cheng, K.; Ok, Y.S. Assembling biochar with various layered double hydroxides for enhancement of phosphorus recovery. *J. Hazard. Mater.* **2019**, *365*, 665–673. [[CrossRef](#)] [[PubMed](#)]

Disclaimer/Publisher’s Note: The statements, opinions and data contained in all publications are solely those of the individual author(s) and contributor(s) and not of MDPI and/or the editor(s). MDPI and/or the editor(s) disclaim responsibility for any injury to people or property resulting from any ideas, methods, instructions or products referred to in the content.